Am J Physiol Cell Physiol 326: C768–C783, 2024.
First published February 5, 2024; doi:10.1152/ajpcell.00444.2023

american physiological society

AMERICAN JOURNAL OF PHYSIOLOGY
CELL PHYSIOLOGY

RESEARCH ARTICLE

Musculoskeletal Biology and Bioengineering

The mechanosensitive gene *arrestin domain containing 2* regulates myotube diameter with direct implications for disuse atrophy with aging

Grant R. Laskin,[1] Ana Regina Cabrera,[2] Nicholas P. Greene,[2] Robert J. Tomko Jr.,[3] Cynthia Vied,[4] and Bradley S. Gordon[1,5]

[1]*Department of of Health, Nutrition, and Food Sciences, Florida State University, Tallahassee, Florida, United States;* [2]*Department of Health, Human Performance and Recreation, Cachexia Research Laboratory, Exercise Science Research Center, University of Arkansas, Fayetteville, Arkansas, United States;* [3]*Department of Biomedical Sciences, Florida State University College of Medicine, Tallahassee, Florida, United States;* [4]*Translational Science Laboratory, Florida State University College of Medicine, Tallahassee, Florida, United States; and* [5]*Institute of Sports Sciences and Medicine, Florida State University, Tallahassee, Florida, United States*

Abstract

Arrestin domain containing 2 and 3 (*Arrdc2/3*) are genes whose mRNA contents are decreased in young skeletal muscle following mechanical overload. *Arrdc3* is linked to the regulation of signaling pathways in nonmuscle cells that could influence skeletal muscle size. Despite a similar amino acid sequence, *Arrdc2* function remains undefined. The purpose of this study was to further explore the relationship of *Arrdc2*/*Arrdc3* expression with changes in mechanical load in young and aged muscle and define the effect of *Arrdc2/3* expression on C2C12 myotube diameter. In young and aged mice, mechanical load was decreased using hindlimb suspension whereas mechanical load was increased by reloading previously unloaded muscle or inducing high-force contractions. *Arrdc2* and *Arrdc3* mRNAs were overexpressed in C2C12 myotubes using adenoviruses. Myotube diameter was determined 48-h posttransfection, and RNA sequencing was performed on those samples. *Arrdc2* and *Arrdc3* mRNA content was higher in the unloaded muscle within 1 day of disuse and remained higher up through 10 days. The induction of *Arrdc2* mRNA was more pronounced in aged muscle than young muscle in response to unloading. Reloading previously unloaded muscle of young and aged mice restored *Arrdc2* and *Arrdc3* levels to ambulatory levels. Increasing mechanical load beyond normal ambulatory levels lowered *Arrdc2* mRNA, but not *Arrdc3* mRNA, in young and aged muscle. *Arrdc2* overexpression only was sufficient to lower myotube diameter in C2C12 cells in part by altering the transcriptome favoring muscle atrophy. These data are consistent with *Arrdc2* contributing to disuse atrophy, particularly in aged muscle.

NEW & NOTEWORTHY We establish *Arrdc2* as a novel mechanosensitive gene highly induced in response to mechanical unloading, particularly in aged muscle. *Arrdc2* induction in C2C12 myotubes is sufficient to produce thinner myotubes and a transcriptional landscape consistent with muscle atrophy and disuse.

aging; electromyostimulation; mechanical overload; mechanical unloading; RNA sequencing

INTRODUCTION

Maintaining functional skeletal muscle mass is critical to human health as loss of muscle increases the risk of morbidity and early mortality (1, 2). Decreasing the mechanical load placed on the muscle for extended periods of time leads to the loss of skeletal muscle mass (disuse atrophy) and increases morbidity and mortality risk (3). Clinically, the elderly are more likely to undergo periods of disuse (e.g., immobilization, hospitalization; 4), which is a problem because aged muscle may waste faster during short-term disuse (5), and the recovery of lost aged muscle upon reloading is slow or absent (6, 7). Therefore, identifying the factors that promote the loss of muscle mass in response to disuse, particularly in the elderly, is needed to develop therapies that preserve muscle mass and prevent debilitating effects to health.

The molecular factors contributing to disuse atrophy may differ between young and aged muscle. For instance, changes to the processes contributing to muscle protein balance in response to hindlimb suspension differ between the limb muscles of young (9 mo) and aged (29 mo) rats (8). Similarly, markers of apoptosis are preferentially induced in the soleus muscle of aged rats in response to disuse relative

Correspondence: B. S. Gordon (bsgordon@fsu.edu).
Submitted 14 September 2023 / Revised 8 January 2024 / Accepted 22 January 2024

to the muscle of young rats (9). Differences to the transcriptional landscape in young and aged muscle in response to disuse may account for some of the age-specific variations to the molecular processes contributing to disuse atrophy. For example, transcripts likely contributing to disuse atrophy such as growth arrest and DNA damage inducible alpha (*Gadd45a*) and histone deacetylase 4 (*Hdac4*) are induced to a greater magnitude in aged muscle in response to hindlimb unloading compared with young muscle (8). Likewise, the mRNA content of regulated in development and DNA damage 2 (*Redd2*) is induced to a higher degree in response to limb immobilization of older rats compared with young rats (10). Thus, it is important to identify age-specific changes to the transcriptional landscape that may preferentially contribute to disuse atrophy in aged muscle.

The α-arrestin family of genes comprises six members termed arrestin domain containing 1–5 (*Arrdc1–5*) and thioredoxin interacting protein (*Txnip/Arrdc6*) (11). Our laboratory previously identified *Arrdc2* and *Arrdc3* as possible mechanically sensitive genes (12). Although the functions of ARRDC2 and ARRDC3 proteins in skeletal muscle are unknown, elevated ARRDC3 protein levels in cancer cells can act as a tumor suppressor by altering pathways such as the Hippo pathway, which is a pathway that can also regulate skeletal muscle size (13, 14). The ARRDC2 amino acid sequences in mice and humans share 52% and 54% homology with their respective ARRDC3 amino acid sequences, and the ARRDC2 protein colocalizes with the β2-adrenergic receptor in HEK293 cells following receptor internalization in a similar manner to ARRDC3 (15), suggesting these proteins may have similar functions. Because ARRDC2 and ARRDC3 appear to be mechanically sensitive and may alter pathways regulating muscle size, the objectives of this study were to define the degree to which *Arrdc2* and *Arrdc3* mRNA are altered in young and aged muscle in response to changes in mechanical load, and to subsequently determine whether manipulating *Arrdc2* and/or *Arrdc3* expression is sufficient to alter muscle size. Our data show that both *Arrdc2* and *Arrdc3* mRNA contents are inversely related to changes in mechanical load, with *Arrdc2* mRNA being more dynamic in response to disuse, particularly in aged muscle. We also show that overexpressing *Arrdc2*, but not *Arrdc3*, results in significantly thinner myotubes in vitro, and the induction of *Arrdc2* results in temporal alterations to the transcriptional landscape reminiscent of disuse atrophy. In all, these data are consistent with *Arrdc2* induction contributing to disuse atrophy, particularly in aged muscle.

MATERIALS AND METHODS

Animals

C57BL/6 mice were purchased from Jackson Laboratories (Bar Harbor, ME), Charles River (Wilmington, MA), or acquired from the National Institute on Aging rodent colony (NIA; Bethesda, MA). All mice were housed in a temperature- (25°C) and light- (12-h light/12-h dark) controlled environment within the vivarium at Florida State University or the University of Arkansas. Mice at Florida State University were provided standard 5001 rodent chow (LabDiet, St. Louis, MO) and water ad libitum until the day of testing. Mice at the University of Arkansas were provided Teklad 8604 rodent chow (Envigo, Indianapolis, IN) and water ad libitum. Animals were euthanized by either cardiectomy or cervical dislocation while under deep isoflurane anesthesia. All animal facilities and experimental procedures were approved by the Institutional Animal Care and Use Committees of Florida State University or the University of Arkansas as appropriate.

Hindlimb Unloading

The mice used in the hindlimb unloading time course were previously described (16). Ten-week-old male and female mice purchased from Jackson Laboratory were randomized to remain ambulatory as a control ($n = 9$ males; $n = 8$ females) or subjected to 1 ($n = 8$ males; $n = 9$ females), 2 ($n = 10$ males; 9 females), 3 ($n = 10$ males; $n = 9$ females), or 7 days ($n = 8$ males; $n = 8$ females) of hindlimb unloading. For hindlimb suspension, the tails were cleaned using ethanol wipes and sterilized with iodine swab sticks before coating the tail with benzoin solution to facilitate tape adhesion. Tails were then wrapped with athletic tape fitted with a loop for the tail suspension apparatus. The tail suspension apparatus was a custom addition to the animal cage, allowing for suspension of the tail by a hook and fishing wire attached to the loop on the mouse tail. The hook and wire were then attached to a swivel system that allowed animals to move freely around the cage using their forelimbs while maintaining hindlimb unloading. Mice were checked daily to ensure food was being consumed and maintenance of general welfare. During hindlimb unloading, food was dampened with tap water to facilitate consumption. At designated time points, animals were deeply anesthetized with 2% isoflurane while avoiding reloading of the hindlimbs. The soleus and gastrocnemius muscles were collected under deep isoflurane anesthesia, snap-frozen in liquid nitrogen, and stored at −80°C until analysis.

Analysis of Publicly Available RNA Sequencing Datasets

The normalized gene counts for mouse/human *Arrdc2/ARRDC2* and *Arrdc3/ARRDC3* were analyzed from two publicly available sets. The first data set from Zhang et al. (17) examined differences in gene expression within the soleus of young (6 mo) and aged (22–24 mo) male C57Bl/6 mice in response to either 10 days of hindlimb unloading ($n = 4$ young; $n = 6$ aged) or 10 days of hindlimb unloading followed by 3 days of reloading ($n = 4$/age), with each condition compared with normal ambulation ($n = 9$/age) (GEO No.: GSE102284). The normalized gene counts for *Arrdc2* mRNA and *Arrdc3* mRNA from all conditions were used for analysis. The second data set from Standley et al. (18) examined the effects of a 10-day pre- to post-bed rest protocol on gene expression within the vastus lateralis of 66- to 67-yr-old males and females with and without β-hydroxy-β-methylbutyrate supplementation (GEO No.: GSE130722). Pre- to post-normalized gene counts for *ARRDC2* mRNA and *ARRDC3* mRNA were analyzed from the nonsupplemented control group only ($n = 6$ males; $n = 3$ females).

Unilateral Electrically Evoked Muscle Contractions

Male C57Bl/6 mice at 3–4 mo of age ($n = 12$; young) or 24–25 mo of age ($n = 7$; aged) were acquired from Charles River

or the NIA aging colony, respectively. Eccentric contractions were induced in the tibialis anterior (TA) muscle via unilateral electrical stimulation of the sciatic nerve under deep isoflurane anesthesia as described by our laboratory (19). Briefly, contractions were initiated via two stainless steel bipolar electrodes inserted subcutaneously near the sciatic nerve. A constant current stimulator (Aurora Scientific, ON, Canada) was used to activate the nerve at a frequency of 100 Hz using a ~20 mA constant current. Each stimulus consisted of 300 pulses with each pulse being 1 ms in duration. The entire protocol consisted of 10 sets of six contractions. Each stimulus within a set was separated by a 10-s rest period and all sets were separated by a 60-s rest period. Following contractions, all mice received a subcutaneous injection of warm saline (600 μL) before returning to their cages where they had free access to water but not food until tissue collection 4-h postcontractions. TA muscles were harvested under deep isoflurane anesthesia, snap-frozen in liquid nitrogen, and stored at −80°C until analysis.

C2C12 Cell Culture

C2C12 myoblasts were purchased from American Type Culture Collection (ATCC) (Cat. No. CRL-1772; Manasses, VA) and cultured subconfluently at 37°C in 5% CO_2 in complete growth media consisting of high glucose Dulbecco's modified Eagle's media (DMEM; Cat. No. 10-017-CV; Corning Life Sciences, Tewksbury, MA) containing 10% fetal bovine serum (FBS; Cat. No. EF-0500-A; Atlas Biologicals, Fort Collins, CO) and 1% penicillin-streptomycin (PS; Cat. No. 15140122; Thermo Fisher Scientific, Waltham, MA). Experiments were conducted in 12-well plates (Cat. No. 10062-894; VWR, Radnor, PA) precoated with a type I rat tail collagen matrix. Coating consisted of diluting RatCol collagen solution (Cat. No. 5056-20ML; Advanced Biomatrix, Carlsbad, CA) and acetic acid into sterile water to a final concentration of 100 μg/mL for rat collagen and 0.1% acetic acid. Five hundred microliters of the final solution were added to each well of the plate and incubated under UV light for 2 h to allow collagen to polymerize. Before plating myoblasts, the collagen solution was aspirated, and wells were rinsed twice with sterile phosphate-buffered saline (PBS). Myotube differentiation was initiated when cells reached ~95% confluence by changing to differentiation media consisting of high glucose DMEM containing 2% horse serum (HS; Cat. No. 16050130; Thermo Fisher Scientific, Waltham, MA), 1% PS, and 1 μM insulin (Cat. No. 11070-73-8; Sigma-Aldrich, Burlington, MA).

Adenovirus Transfection and Myotube Diameter

C2C12 myoblasts were differentiated for 3 days. Differentiation was confirmed by the presence of multinucleated mature myotubes covering the wells. After confirmation, C2C12 myotubes were transfected using adenoviruses obtained from Vector Biolabs (Malvern, PA) encoding *Arrdc2* + *Gfp* (Ad-GFP-m-ARRDC2[cop];), *Arrdc3* + *Gfp* (Ad-GFP-m-ARRDC3), a combination of both *Arrdc2* + *Gfp* & *Arrdc3* + *Gfp* vectors or adenovirus encoding only *Gfp* as a control (Ad-CMV-GFP; Cat. No. 1060). Adenoviruses encoding *Arrdc2* and *Arrdc3* were custom made for our laboratory by Vector Biolabs. The adenovirus encoding *Arrdc2* was codon optimized (i.e., [cop]) to minimize gene recombination during virus production. The expression of all genes was driven by cytomegalovirus (CMV) promoters with *Arrdc2/3* and *Gfp* driven by separate CMV promoters within the same viral vector. Transfection consisted of adding the adenovirus directly to the differentiation media at final viral concentrations of 3.2×10^8 PFU/mL of media, 1.6×10^8 PFU/mL of media, and 8.0×10^7 PFU/mL of media for the *Arrdc2* + *Gfp*, *Arrdc3* + *Gfp*, and *Gfp* only vectors, respectively. The combination of the *Arrdc2* + *Gfp* & *Arrdc3* + *Gfp* vectors was at a viral concentration of 1.6×10^8 PFU/mL of media for each vector. The viral concentration used in the experiments was that which produced the highest transfection efficiency (e.g., highest number of GFP-positive myotubes) while maintaining cell viability. Western blot analysis showed GFP protein levels were similar across transfection conditions (data not shown). Virus-containing media was changed 24 h after transfection to fresh differentiation media for experiments lasting 48 h. Twenty-four- or 48-h posttransfection, nonoverlapping myotube images from the entire well were acquired at ×200 on a Leica DMi8 microscope (Wetzler, Germany) mounted with a Leica DFC7000 T camera using Leica Application Suite X software. Light and fluorescent images were concurrently taken. To circumvent fluorescent interference from cellular debris and/or undifferentiated myoblasts, myotube diameter was measured on the light image with the fluorescent image used to identify GFP-positive myotubes for measurement. Only GFP-positive myotubes with an elongated, mature, nonnascent morphology were analyzed (visualization is found in Ref. 20). Myotube diameter was calculated by taking an average of five points along the length of the myotube. Diameter was determined by an investigator blinded to the transfection conditions using ImageJ software (NIH, Bethesda, MD). Cells were harvested in 500 μL TRI reagent (Zymo Research, Irvine, CA) for subsequent RNA analysis. All C2C12 myotube diameter experiments consisted of three independent experimental replicates, with the value of the mean diameter of all myotubes from each independent replicate used in the analysis. The mean diameter of *Arrdc2*, *Arrdc3*, or *Arrdc2* + *Arrdc3* transfected wells was normalized to the mean diameter of the corresponding *Gfp* transfected well within the corresponding replicate with the normalized values used in the final analysis. The C2C12 myotube experiments used for gene expression analysis consisted of three independent experimental replicates. Gene expression was assessed relative to the *Gfp* only condition within each experimental replicate, and the gene expression fold changes from each replicate were averaged to generate the final data set. We transfected more wells with *Arrdc2* and *Arrdc3* than *Gfp* for each independent replicate used in gene expression analysis because of a limited quantity of *Gfp* adenovirus. No samples/wells were removed due to outlying values in gene expression.

Analyses of Protein-Protein Interaction Networks and Predicted Transcription Factor Binding Sites

Human and mouse ARRDC2 proteins were analyzed in the Search Tool for Retrieval of Interacting Genes/Proteins (STRING) database (string-db.org) to generate potential protein-protein interaction networks and retrieve respective amino acid sequences (21). *K*-means clustering was applied to the networks to identify three clusters of similar protein

function. Predicted transcription factor binding sites within a gene promoter were defined by inputting gene names into EnhancerDB (lcbb.swjtu.edu.cn/EnhancerDB) (22). Transcription factor binding sites ≤5,000 bp upstream from the transcription start site were assessed.

Secondary Structure Prediction and Protein Homology Modeling

Secondary structure and disorder predictions were performed using the PSIPred server (bioinf.cs.ucl.ac.uk/psipred/) (23). Homology modeling was carried out using the default settings on Phyre2 (sbg.bio.ic.ac.uk/phyre2/html/page.cgi?id=index) (24) and AlphaFold2 (accessed via colab.research.google.com/github/sokrypton/ColabFold/blob/main/AlphaFold2.ipynb) (25) and executed in Jupyter notebook (jupyter.org) using the default settings. The best-rated models were exported as pdf files and visualized using ChimeraX (cgl.ucsf.edu/chimerax/). The Phyre2 and AlphaFold2 models were superimposed using the Matchmaker command in ChimeraX, and the root mean square deviation (RMSD) between the models was calculated using the RMSD command.

RNA Extraction, cDNA Synthesis, and qRT-PCR

RNA from the hindlimb unloading time course was isolated and cDNA synthesized as described by Rosa-Caldwell et al. (16). For the muscle contractions experiment, ~20 mg of TA muscle was homogenized in 500–600 μL of Zymo Tri Reagent (Irvine, CA). The RNA from homogenized muscle or C2C12 myotubes was isolated using a Zymo Direct-zol RNA Miniprep kit with on-column DNase treatment (Irvine, CA; Cat. No. R2050). RNA quantity and purity were determined spectrophotometrically by the 260- to 280-nm ratio. cDNA was synthesized from 1 to 1.75 ng of RNA using a high-capacity cDNA reverse transcription kit (Thermo Fisher Scientific, Waltham, MA; Cat. No. 4368814). qRT-PCR was conducted on either a QuantStudio3, QuantStudio7 (both from Thermo Fisher Scientific, Waltham, MA), or CFX Connect thermal cycler (Bio-Rad Laboratories, Hercules, CA) using PowerUp SYBR Green master mix (Cat. No. A25742; Thermo Fisher Scientific, Waltham, MA) or TaqMan fast advanced master mix (Cat. No. 4444557; Applied Biosystems, Foster City, CA). The conditions for qRT-PCR with SYBR Green were an initial 2 min at 50°C and 2 min at 95°C, followed by 40 cycles with each cycle consisting of a 15-s denature step at 95°C, a 15-s annealing step at 55°C, and a 1-min extension step at 72°C. A melt curve analysis was performed for each primer pair to ensure that a single product was amplified, and the product sizes for each primer pair were verified via agarose gel electrophoresis before analysis. The conditions for TaqMan were an initial 2 min at 50°C and 10 min at 95°C, followed by 45 cycles with each cycle consisting of a 15-s denature step at 95°C, a 1-min annealing step at 60°C, and a 1-min extension step at 60°C. Relative expression levels of each target gene were normalized using the $\Delta\Delta C_t$ method with *Rplp0* as the reference genes for high force contraction and *Arrdc2* transfection experiments (analyzed at Florida State University) or *18s* (ID No.: Mm03928990_g1) for the hindlimb unloading time course (analyzed at University of Arkansas) as neither *Rplp0* nor *18s* mRNA contents were altered by those treatments. It is unlikely that using these different reference genes would alter the conclusions since both genes were stable across those treatments. *Gadph* was used as the reference gene for *Arrdc3* experiments because it was more stable than *Rplp0* in those particular experiments. myostatin (*Mstn*) was measured using TaqMan primer probes (ID No.: Mm01254559_m1). The primer sequences for SYBR Green reactions are shown in Table 1.

RNA Sequencing

Total RNA extracted from myotubes overexpressing *Arrdc2* or expressing *Gfp* within an experimental replicate was subjected to RNA sequencing. A next generation sequencing library was prepared for each sample using NEBNext Poly(A) mRNA Magnet Isolation Module followed by NEBNext Ultra II Directional RNA Library Kit for Illumina. Libraries were barcoded for multiplexing with NEBNext Multiplex Oligos for Illumina. Each multiplexed library was sequenced as a paired-end, 50 base pair sequencing run on an Illumina NovaSeq 6000, located in the Translational Science Laboratory at Florida State University College of Medicine. Adapter trimming was performed as part of individual library demultiplexing. Quality control analysis of each library was performed using fastQC (bioinformatics.babraham.ac.uk/projects/fastqc/). Star aligner (26) was used for mapping and alignment of the raw reads to the mouse genome (current version, GRCM39), generating counts for each gene. DESeq2 (27) was used to determine statistically significant differentially expressed genes (DEGs) in *Arrdc2* overexpressing myotubes relative to *Gfp*

Table 1. *SYBR Green primer sequences*

Gene Symbol	Forward (5′-3′)	Reverse (5′-3′)	Amplicon Size, bp
Rplp0	CAACCCAGCTCTGGAGAAAC	GTTCTGAGCTGGCACAGTGA	169
Arrdc2	TCTCCCTGGTGACATCCTTC	CACGTGTGCAGTACCAGGAT	204
*Arrdc2[cop]**	GATTCCCATTTTCGCTGAGA	CCATCAACACTTGCAACCAC	135
Arrdc3	CCGGCTCCAATACTGCCTATAC	GCCTTCGAATGAGGTAGCAA	194
Myogenin	TGCCCAGTGAATGCAACTC	ATATCCTCCACCGTGATGCT	166
Mafbx	GTCGCAGCCAAGAAGAGAAAG	ACTCAGGGATGTGAGCTGTGA	240
Murf1	AAGCAGGAGTGCTCCAGTCG	ACCAGCATGGAGATGCAGTTA	217
Redd1	TGGTGCCCACCTTTCAGTTG	GTCAGGGACTGGCTGTAACC	121
Redd2	CCAGCCTCAAGGACTTCTTC	TCTTCAATGACTGTCGTTCC	133
Bnip3	AGCTTTGGCGAGAAAAACAG	TGAGAGTAGCTGTGCGCTTC	175
Hspa1a	TGGTGCTGACGAAGATGAAG	ATGATCCGCAGCACGTTTAG	154
Gadph	GTTGTCTCCTGCGACTTCA	TGCTGTAGCCGTATTCATTG	124

Arrdc2/3, arrestin domain containing 2 and 3; *Bnip3*, BCL2 interacting protein 3; *Hspa1a*, heat shock protein 70 kDa; *Mafbx*, muscle atrophy F-box; *murf1*, muscle RING-finger protein-1; *Redd1*, regulated in development and DNA damage 1; *Redd2*, regulated in development and DNA damage 2. *Used to detect codon optimized *Arrdc2* mRNA following Ad-GFP-m-ARRDC2[cop] transfection.

expressing myotubes. These steps yielded lists of DEGs with a false discovery rate of $P < 0.05$ (adj. P value) and a measure of confidence of the difference for each comparison. The raw data from the RNA sequencing analysis are publicly available in GEO (No. GSE248869).

Functional Gene Enrichment and Prediction of Regulatory Transcription Factors

Upregulated and downregulated DEGs in *Arrdc2* overexpressing myotubes were uploaded into the Database for Annotation, Visualization, and Integrated Discovery (DAVID; david.ncifcrf.gov) software to define the most enriched Kyoto Encyclopedia of Genes and Genomes (KEGG) pathways (28). DEGs were included in the upregulated or downregulated list if they had significant adjusted P values ≤ 0.05. A fold change threshold for inclusion was not applied (29, 30). The top 500 DEGs (based upon adjusted P values) from both upregulated and downregulated gene lists were then uploaded into Landscape in silico deletion analysis (LISA; lisa.cistrome.org/) software to identify predicted transcription factors regulating each gene list (31).

Statistical Analysis

Two-way ANOVA was used to evaluate *Arrdc2* and *Arrdc3* mRNA across time in response to hindlimb suspension using unloading and sex as the two factors. Two-way ANOVA was also used to evaluate the effects of unloading/reloading and muscle contractions on *Arrdc2* and *Arrdc3* mRNA in young and aged mouse muscle using age and loading or age and contractions as the two factors, respectively. Tukey's multiple comparisons test was used post hoc to assess specific pairwise comparisons if an interaction was observed. Paired Student's t tests were used to evaluate changes in *ARRDC2* and *ARRDC3* mRNA content in the human RNA sequencing data set. RNA sequencing analysis in the C2C12 myotubes was described earlier. One-way ANOVA was used to evaluate changes in normalized myotube diameter across transfection conditions with Dunnett's multiple comparisons test used post hoc. Unpaired Student's t tests were used to compare normalized myotube diameter at 24 h and gene content between transfection conditions. All analyses were performed using GraphPad Prism Software (v.10, La Jolla, CA). Significance was set at $P \leq 0.05$ for all analyses. All data are presented as means ± SD, as individual data points superimposed onto either box-and-whiskers plots or the means ± SD, or as paired points connected by a line.

RESULTS

Arrdc2 and Arrdc3 mRNA Contents Are Higher in Young and Aged Skeletal Muscle in Response to Mechanical Unloading, with the Induction of Arrdc2 mRNA Being More Pronounced, Especially in Aged Muscle

As previously reported (16), soleus mass was 38.6% and 33.8% lower and gastrocnemius mass was 15.7% and 17.5%

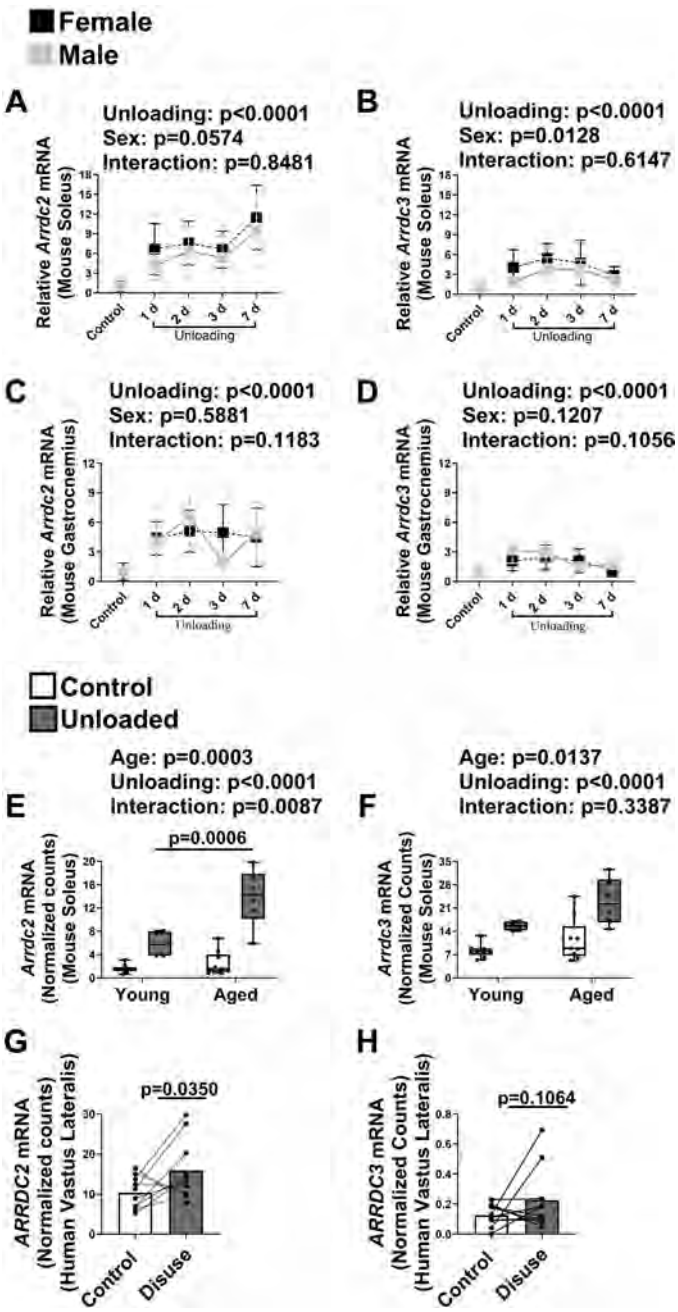

Figure 1. The mRNA content of arrestin domain containing (*Arrdc)2* and *Arrdc3* are induced in muscle in response to mechanical unloading. The relative mRNA content of *Arrdc2* (*A* and *C*) and *Arrdc3* (*B* and *D*) were assessed in the soleus and gastrocnemius of male and female mice across 7 days of hindlimb unloading by qRT-PCR. Data are relative to the control condition within each sex. Control timepoint contains $n = 9$ male and $n = 8$ female mice, 1-day unloading timepoint contains $n = 8$ male and $n = 9$ female mice, 2-day unloading timepoint contains $n = 10$ male and $n = 9$ female mice, 3-day unloading time point contains $n = 10$ male and $n = 9$ female mice, and 7-day unloading timepoint contains $n = 8$ male and $n = 8$ female mice. Data were analyzed by two-way ANOVA. The normalized counts of *Arrdc2* (*E*) and *Arrdc3* (*F*) mRNAs in the soleus of young ($n = 9$ control; $n = 4$ unloaded) and aged ($n = 9$ control; $n = 6$ unloaded) mice in response to 10 days of hindlimb unloading were acquired from a published RNA sequencing dataset (17) and analyzed by two-way ANOVA. Line connecting plots represents significance by Tukey's post hoc. The normalized mRNA counts of *ARRDC2* (*G*) and *ARRDC3* (*H*) mRNAs in the vastus lateralis of older humans ($n = 10$) before and after 10 days of bedrest were acquired from a published RNA sequencing data set (18) and analyzed by paired Student's t test. Data are presented as means ± SD, individual data points superimposed upon box-and-whisker plots, or paired data points connected by a line.

lower in male and female mice, respectively, after 7 days of unloading compared with the sex-matched ambulatory control values. In both sexes and muscles, there were main effects of unloading for *Arrdc2* mRNA ($P < 0.0001$) and *Arrdc3* mRNA ($P < 0.0001$) contents to be higher in the soleus and gastrocnemius throughout the 7-day unloading time course (Fig. 1, *A–D*). In the soleus, the *Arrdc2* mRNA induction approached significance for a sex effect ($P = 0.0574$) whereas *Arrdc3* mRNA induction was different between sexes (Sex: $P = 0.0128$), a finding consistent with sex impacting the molecular response to disuse (16). There were no sex effects in the gastrocnemius for *Arrdc2* ($P = 0.5881$) or *Arrdc3* ($P = 0.1207$). In both soleus and gastrocnemius (regardless of sex), the mean fold change for *Arrdc2* mRNA in response to unloading was significantly greater than the mean fold change for *Arrdc3* mRNA ($P < 0.0001$). Our laboratory previously showed *Arrdc2* and *Arrdc3* levels were induced by food deprivation (12). Food consumption could not be accurately assessed during the hindlimb suspension time course because the food was dampened to make consumption easier. Therefore, it is possible that some food restriction could have contributed to the *Arrdc2/3* inductions in response to the hindlimb suspension. Analysis of a publicly available RNA sequencing data set (17) from young (6 mo) and aged (22–24 mo) mice subjected to 10 days of hindlimb unloading showed *Arrdc2* and *Arrdc3* mRNA contents were higher in the soleus of young and aged mice in response to unloading compared with age-matched ambulatory control values (Unloading: $P < 0.0001$; Fig. 1, *E* and *F*). The magnitude of *Arrdc2* induction was more pronounced in aged muscle than young muscle in response to unloading (Interaction: $P = 0.0087$) with pairwise comparison showing *Arrdc2* mRNA content was higher in aged muscle subjected to unloading compared with the young muscle subjected to unloading ($P = 0.0006$). There was no significant interaction observed for *Arrdc3* mRNA ($P = 0.3387$). Consistent with the unloading time course data, the magnitudes of change for *Arrdc2* mRNA in the young and aged soleus were greater than the magnitudes for *Arrdc3* mRNA ($P \leq 0.0029$). Characteristics of the muscles from those young and aged mice used to generate the RNA sequencing data set are previously reported (17). Analysis of a publicly available human RNA sequencing data set (18) generated from the vastus lateralis of 66- to 67-yr-old males and female humans showed *ARRDC2* mRNA content was significantly higher in response to 10 days of bedrest relative to pre-bedrest values ($P = 0.0350$, Fig. 1*G*). *ARRDC3* mRNA was numerically higher in response to bedrest, although the increase was not significant ($P = 0.1064$, Fig. 1*H*).

The Degree of Mechanical Load Placed on Young and Aged Muscle is Directly Related to Changes in Arrdc2 mRNA Content, but Only Partially Related to Changes in Arrdc3 mRNA Content

Combining reloading data from the mouse RNA sequencing data set into Fig. 1, *E* and *F* analyses still showed a main effect of loading status for *Arrdc2* and *Arrdc3* mRNA to change in both young and aged muscle (Loading: $P < 0.0001$, Fig. 2, *A* and *B*). In aged muscle, *Arrdc2* mRNA was

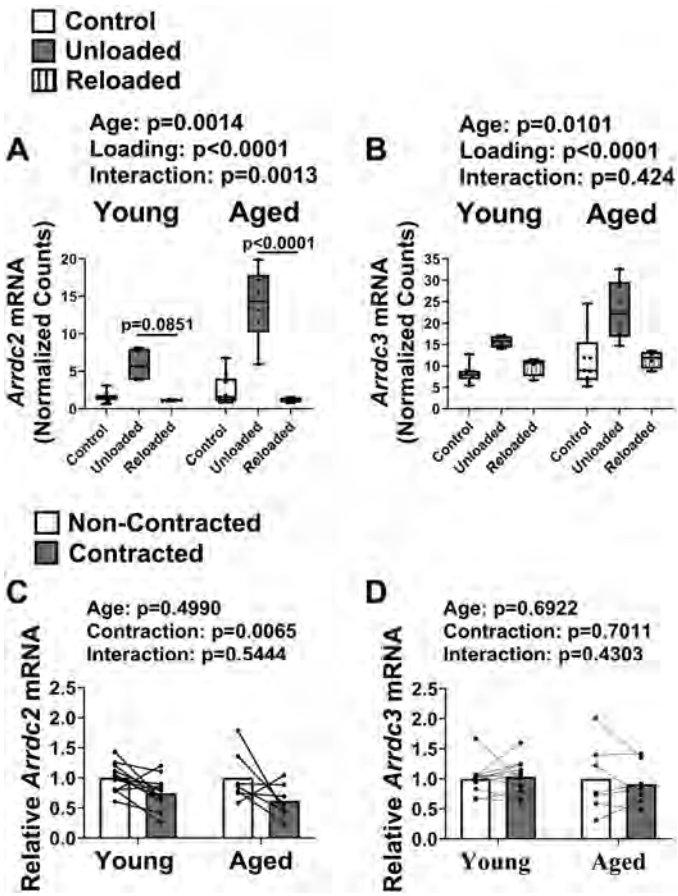

Figure 2. Arrestin domain containing (*Arrdc*)*2* and *Arrdc3* mRNA content in young and aged muscle are maintained at low levels when mechanical load is applied to the muscle. The normalized mRNA counts of *Arrdc2* (*A*) and *Arrdc3* (*B*) in the soleus muscle from young and aged mice subjected to normal ambulation ($n = 9$/age), 10 days of hindlimb unloading ($n = 4$ young; $n = 6$ aged), or 10 days of hindlimb unloading plus 3 days of reloading ($n = 4$/age) were acquired from a publicly available RNA sequencing data set (16) and analyzed by two-way ANOVA with Tukey's multiple comparisons used post hoc. Line connecting plots represent significance by Tukey's post hoc. The relative mRNA content of *Arrdc2* (*C*) and *Arrdc3* (*D*) in the tibialis anterior (TA) muscle of young ($n = 12$) and aged ($n = 7$) mice subjected to unilateral high force muscle contractions was assessed by qRT-PCR. Data are relative to the noncontracted muscle within each age as the relative content of each gene for young and aged mice was determined in separate qRT-PCR reactions. Data analyzed by two-way ANOVA. Data are presented as individual data points superimposed on box-and-whisker plots or paired data points connected by a line.

lowered to a greater magnitude in response to reloading compared with young muscle (Interaction: $P = 0.0013$) with pairwise comparisons showing *Arrdc2* mRNA was significantly lower in the reloaded aged soleus compared with unloaded aged soleus ($P < 0.0001$, Fig. 2*A*). The *P* value for *Arrdc2* mRNA to be lower in reloaded young soleus compared with unloaded young soleus approached significance ($P = 0.0851$, Fig. 2*A*). Moreover, increasing the mechanical load beyond normal ambulatory levels via high force contractions lowered *Arrdc2* mRNA content in the TA muscles of young and aged mice below ambulatory values (Contraction: $P = 0.0065$, Fig. 2*C*). *Arrdc3* mRNA content was not affected by contractions in young or old muscle when measures were made in the freely fed state (Contraction: $P = 0.7011$, Fig. 2*D*).

The Diameter of C2C12 Myotubes Overexpressing Arrdc2, but Not Arrdc3, is Thinner than Control Myotubes

Because *Arrdc2* and *Arrdc3* mRNA content appear to be regulated by changes in mechanical load, particularly unloading, we sought to determine the effect of *Arrdc2* and *Arrdc3* induction on muscle size by transfection of adenoviral vectors encoding *Arrdc2* + *Gfp*, *Arrdc3* + *Gfp*, a combination of those two vectors, or *Gfp* only as a control into C2C12 myotubes. Forty-eight hours posttransfection, a significant ANOVA *F* value was observed for normalized myotube diameter ($P = 0.0003$, Fig. 3*A*) with pairwise comparisons showing the normalized diameter of C2C12 myotubes overexpressing *Arrdc2* and *Arrdc2* + *Arrdc3* were 8.8% and 12.7% thinner, respectively, compared with myotubes transfected with *Gfp* only ($P = 0.0033$ and $P = 0.0003$, respectively; Fig. 3*A*). In contrast, the normalized diameter of myotubes overexpressing *Arrdc3* was not different than *Gfp* control myotubes ($P = 0.7805$, Fig. 3*A*). Attempts to measure ARRDC2 and ARRDC3 protein levels in transfected cells were not successful due to lack of valid antibodies. Transfection resulted in a ~1,000-fold increase in the contents of codon optimized *Arrdc2* mRNA or *Arrdc3* mRNA relative to endogenous *Arrdc2/Arrdc3* mRNA levels in *Gfp* controls. *Arrdc2* induction lowered endogenous *Arrdc3* mRNA compared with *Gfp* transfected myotubes whereas *Arrdc3* induction did not affect endogenous *Arrdc2* mRNA levels (data not shown).

Analysis of Predicted ARRDC2 Protein-Protein Interactions and ARRDC2 Protein Structural Elements Suggests ARRDC2 May Regulate Gene Transcriptional Pathways

We used the Search Tool for the Retrieval of Interacting Genes/Proteins (STRING) to identify possible proteins that may interact/function with ARRDC2 (21). Protein-protein interaction network for human and mouse ARRDC2 using *k*-means clustering identified a common cluster in both species containing members of the neuronal precursor cell-expressed developmentally downregulated 4 (NEDD4) subfamily of proteins (NEDD4 and NEDD4-like [NEDD4L]; Supplemental Fig. S1, *A* and *B*, boxed area). NEDD4 is a WW domain-containing HECT E3 ubiquitin ligase that contributes to muscle atrophy induced by mechanical unloading (e.g., hindlimb suspension, denervation) (32, 33) at least in part by altering transcription factor activity via ubiquitylation. WW domain-containing proteins interact with proteins containing PPxY motifs and the human ARRDC2 amino acid sequence contains two characteristic PPxY motifs (amino acids 339–342 and 384–388 in human ARRDC2) conserved across mice and rats (Fig. 4*A*). Secondary structure predictions and homology modeling of human ARRDC2 using two complementary structure prediction engines (Phyre2 and AlphaFold2) predicts the PPxY motifs lie within intrinsically disordered regions (Fig. 4, *B* and *C*). Both homology engines confidently identified the characteristic arrestin fold with a root mean square deviation across the domain of ~1.1 Å (Fig. 4, *D–F*), and again placed the PPxY motifs in disordered regions that are surface exposed as is common for PPxY motifs (34) suggesting they are likely to be functional (note Phyre2 did not confidently model residues 384–388).

Arrdc2 Overexpression for 48 h Produces a Myotube Gene Expression Signature Reminiscent of Disuse Muscle Atrophy

Given the potential for ARRDC2 to interact with proteins that regulate gene expression, we measured the mRNA contents of the canonical atrophy related genes muscle atrophy F-box (*Mafbx*), myogenin (*Myog*), and muscle RING-finger

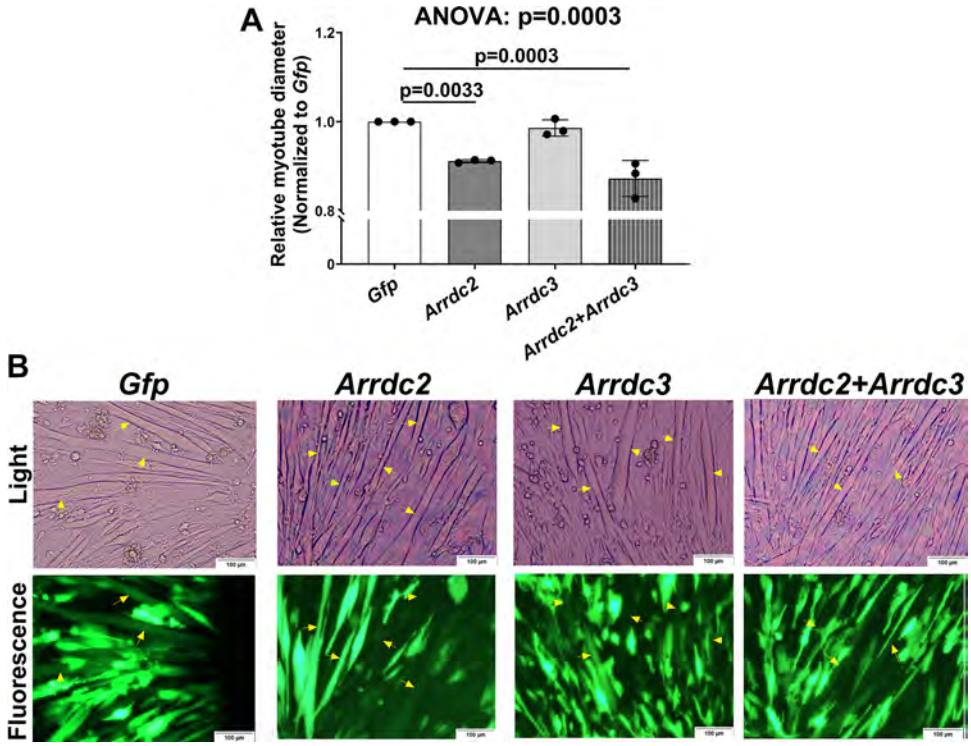

Figure 3. Arrestin domain containing (*Arrdc*)*2* overexpression lowers C2C12 myotube diameter 48-h posttransfection. *A*: The normalized diameter of myotubes overexpressing *Arrdc2*, *Arrdc3*, or *Arrdc2* + *Arrdc3* was compared with the normalized diameter of myotubes expressing *Gfp* only. *B*: representative light and fluorescent images of each transfection condition. Yellow arrows indicate GFP-positive, mature myotubes. $n = 148–239$ myotubes analyzed from each transfection condition generated from three independent experimental replicates. Data analyzed by one-way ANOVA with Dunnett's multiple comparisons post hoc. Lines connecting bars indicates significance by Dunnett's post hoc. Data are presented as three individual data points representing the normalized mean of each independent experimental replicate ± SD.

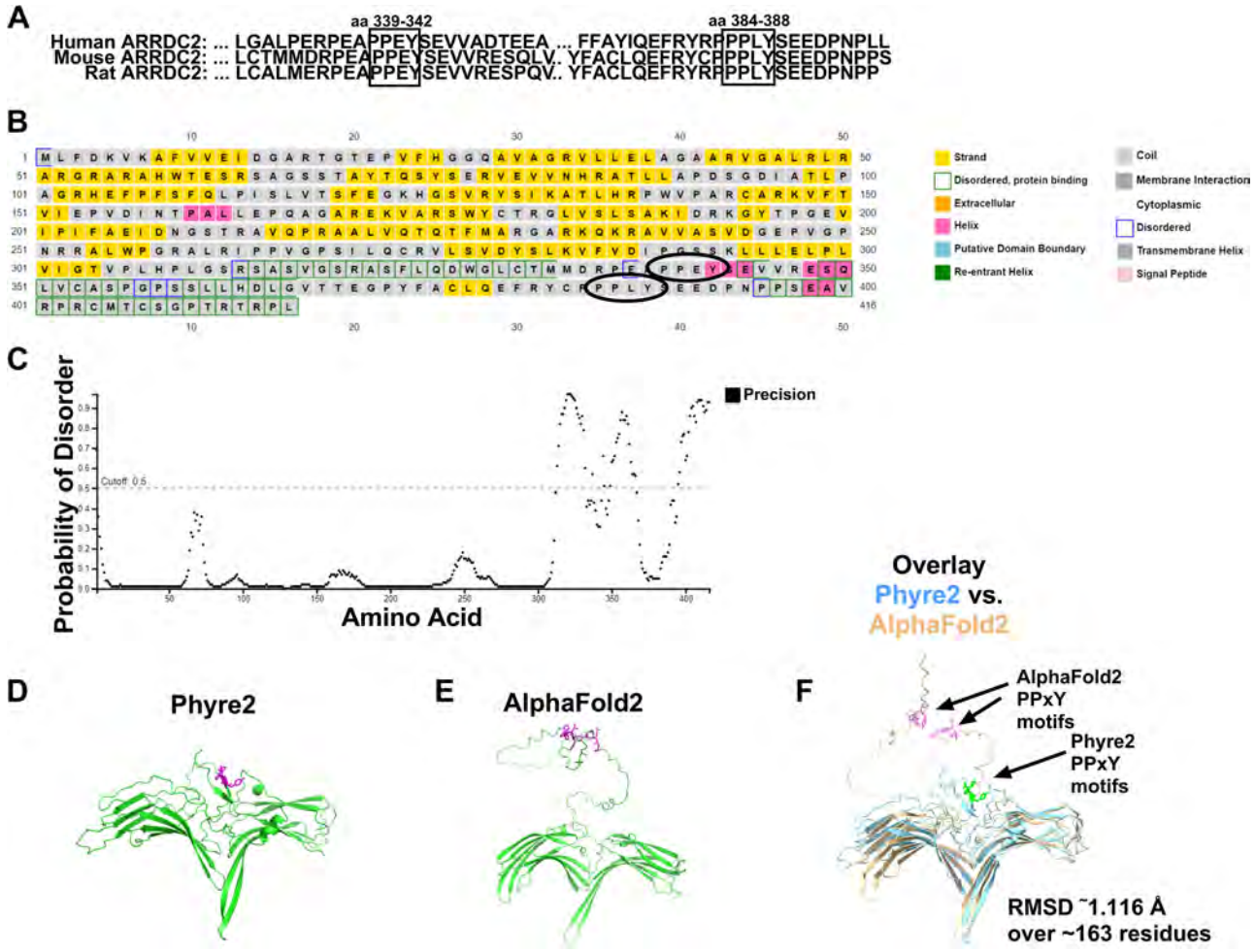

Figure 4. Structural analysis of arrestin domain containing 2 (ARRDC2) protein. The sequence alignment of putative PPxY motifs located in the C-terminus of human, mouse, and rat ARRDC2 (*A*). Amino acid residues shown in the boxes are numbered according to the human sequence. Predictions of secondary structure (*B*) and disorder for human ARRDC2 (*C*). Positions of the putative PPxY motifs are circled in the secondary structure plot. Homology models of human ARRDC2 produced using Phyre 2 (*D*) and AlphaFold2 (*E*) are shown in ribbon model with residues of the putative PPxY motifs rendered in pink using stick model. *F*: superimposition of the Phyre2 (cyan) and AlphaFold2 (gold) models is shown, with the positions of the putative PPxY motifs indicated in stick model. Although the positioning of the motifs differs between the two models, both place the motifs in poorly ordered regions of the structure poised for protein-protein interaction, consistent with the secondary structural (*B*) and disorder (*C*) predictions for ARRDC2 and the known functions of PPxY motifs. The root mean square deviation (RMSD) between the two models over 163 amino acids comprising the arrestin C-terminal-like domain is shown.

protein-1 (*Murf1*) as their mRNA contents are controlled by transcription factors that can be regulated by the NEDD4 subfamily (35, 36). Consistent with a gene transcription regulatory function, the mRNA contents of *Mafbx* and *Myog* were higher in myotubes overexpressing *Arrdc2* relative to *Gfp* control myotubes at 48-h posttransfection ($P = 0.0013$ and $P = 0.0017$, respectively; Fig. 5, *A* and *B*). However, *Murf1* mRNA content was not different between *Arrdc2* overexpressing and *Gfp* expressing myotubes ($P = 0.2222$, Fig. 5*C*). In silico analysis of the *Mafbx*, *Myog*, and *Murf1* promoters with EnhancerDB (22) was used to define transcription factors with predicted binding sites common to *Mafbx* and *Myog*, but not *Murf1*. A total of 73 transcription factors common to *Mafbx* and *Myog* were identified (Supplemental Table S1), including forkhead box O3 (FOXO3), a known regulator of disuse atrophy (37). Regulated in development and DNA damage 1 (*Redd1*) and *Redd2* are regulated in part by FOXO3 and are induced in response to disuse (38). Accordingly, *Redd1* and *Redd2* mRNA contents were also higher in myotubes overexpressing *Arrdc2* compared with *Gfp* control myotubes ($P = 0.0069$ and $P < 0.0001$, respectively; Fig. 5, *D* and *E*). Although myotube diameter was not affected 48 h following *Arrdc3* transfection, *Mafbx* mRNA content was higher in *Arrdc3* overexpressing myotubes compared with *Gfp* myotubes ($P < 0.0001$, Fig. 5*F*). Unlike *Arrdc2* overexpressing myotubes, *Arrdc3* induction did not alter the mRNA contents of *Myog*, *Redd1*, or *Redd2* ($P = 0.1667$, $P = 0.4266$, and $P = 0.2776$, respectively; Fig. 5, *G*, *I*, and *J*). The mRNA content of *Murf1* was lower in *Arrdc3* overexpressing myotubes ($P = 0.0017$, Fig. 5*H*).

RNA sequencing was then used to define ARRDC2-mediated changes to the transcriptome at the 48-h time point. *Arrdc2* induction in myotubes altered the content of 4,362 genes (2,039 upregulated and 2,323 downregulated) compared with *Gfp* control myotubes (Fig. 6*A*; Supplemental Tables S2 and S3), including those genes identified in Fig. 5.

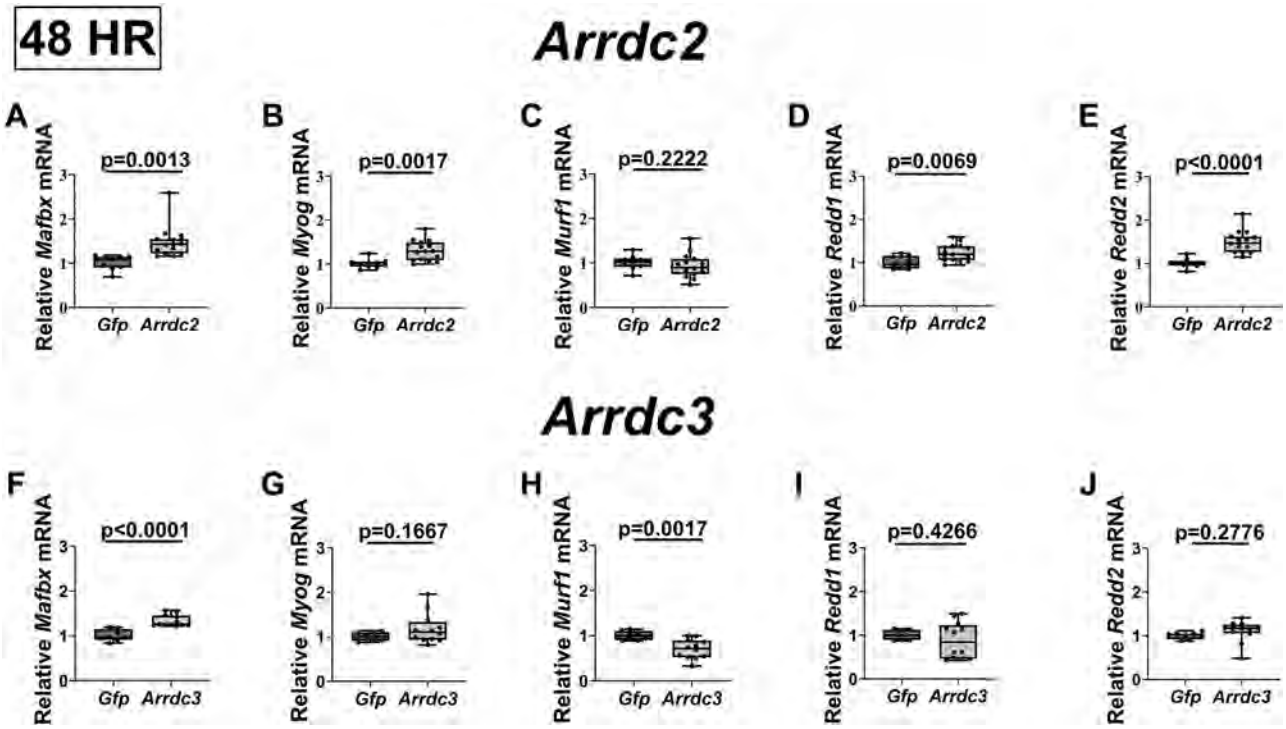

Figure 5. Arrestin domain containing 2 (*Arrdc2*) induction alters content of genes related to muscle atrophy. *A–E*: changes in C2C12 myotube gene expression 48-h post-*Arrdc2* transfection ($n = 15$ wells) compared with *Gfp* transfection ($n = 9$ wells). The relative mRNA content of muscle atrophy F-box (*Mafbx*, *A*), myogenin (*Myog*, *B*) muscle RING-finger protein-1 (*Murf1*, *C*), regulated in development and DNA damage 1 (*Redd1*, *D*), and *Redd2* (*E*) were assessed in C2C12 myotubes by qRT-PCR at 48-h posttransfection. *F–J*: changes in C2C12 myotube gene expression 48-h post-*Arrdc3* transfection ($n = 12$ wells) compared with *Gfp* transfection ($n = 8$ wells). The relative mRNA content of *Mafbx* (*F*), *Myog* (*G*), *Murf1* (*H*), *Redd1* (*I*), and *Redd2* (*J*) were assessed in C2C12 myotubes by qRT-PCR at 48-h posttransfection. Data are relative to *Gfp* control values and generated from three independent experimental replicates. Data analyzed by unpaired Student's *t* tests. *P* values for each comparison are shown on each panel. Data are presented as individual data points superimposed on box-and-whisker plots.

The top 200 most significant upregulated genes by adjusted *P* value in *Arrdc2* expressing myotubes included Caspase-3 (*Casp3;* adj. $P < 0.0001$, Fig. 6*B*), BCL2 interacting protein 3 (*Bnip3*; adj. $P < 0.0001$, Fig. 6*C*) and myostatin (*Mstn;* adj. $P < 0.0001$, Fig. 6*D*), which are transcripts commonly induced in response to muscle disuse and which contribute to cellular processes altering muscle size (39–42). Among the 200 most significant downregulated genes by adjusted *P* value in *Arrdc2* expressing myotubes were *Hspa1a* and *Hspa1b* which encode heat shock protein 70 kDa (adj. $P < 0.0001$, Fig. 6, *E* and *F*) and the transcription factor *Myc* (adj. $P < 0.0001$, Fig. 6*G*), with all those genes implicated in the regulation of muscle mass and whose expression decreases in response to unloading (30, 43, 44).

The five most highly enriched KEGG pathways associated with upregulated genes were lysosome, cell cycle, metabolic pathways, fatty acid metabolism, and p53 signaling pathway (Fig. 7*A*; Supplemental Table S4). Included within the categories of lysosome and p53 signaling pathways were genes encoding cathepsin A (*Ctsa;* adj. $P = 0.0162$, Fig. 7*B*), cathepsin O (*Ctso*; adj. $P < 0.0001$, Fig. 7*C*), caspase-8 (*Casp8*, adj. $P = 0.0324$, Fig. 7*D*), and caspase-9 (*Casp9;* adj. $P < 0.0001$, Fig. 7*E*), which collectively are proteases involved with protein degradation (45, 46). Genes within cell cycle included histone deacetylase 1 (*Hdac1*; adj. $P = 0.0453$, Fig. 7*F*), which can promote atrophy-related gene expression (47), as well as cyclin-dependent kinase inhibitor 1B/p27 (*Cdkn1b*; adj. $P < 0.0001$, Fig. 7*G*) and cyclin-dependent kinase inhibitor 1C/p57 (*Cdkn1c*; adj. $P < 0.0001$, Fig. 7*H*), which encode members of the CDK interacting protein/kinase inhibitory protein (Cip/Kip) family that has been implicated in the regulation of translational capacity (48). Analysis of the 500 most significant upregulated genes by adjusted *P* value using LISA software predicted myoblast determination protein 1 (MYOD1), MYOG, Spi-1 proto-oncogene (SPI1), GATA-binding factor 2 (GATA2), and yes-associated protein 1 (YAP1) as transcription factors likely to influence the upregulated gene set (Fig. 7*I*; Supplemental Table S5).

Repeating the same analyses with the list of downregulated genes identified ribosome biogenesis in eukaryotes, nucleocytoplasmic transport, ribosome, spliceosome, and proteosome as the five most highly enriched KEGG categories (Fig. 8*A*; Supplemental Table S6). Included within the categories of ribosome biogenesis in eukaryotes, nucleocytoplasmic transport, and ribosome were fibrillarin (*Fbl*; adj. $P = 0.0007$, Fig. 8*B*) and NMD3 ribosome export adaptor (*Nmd3*; adj. $P < 0.0001$, Fig. 8*C*), which regulate the nuclear export of the ribosome (49), and nucleolar protein 5A (*Nop56*; adj. $P < 0.0001$, Fig. 8*D*), which is involved in processing of rRNAs (50). Also included were eukaryotic initiation factor 6 (*Eif6*; adj. $P = 0.0007$, Fig. 8*E*), DEAD-box helicase 19B (*Ddx19b*; adj. $P = 0.0015$, Fig. 8*F*), and ribosomal L24 domain containing 1 (*Rsl24d1*; adj. $P = 0.0006$, Fig. 8*G*) that regulate the activity and/or function of the ribosome

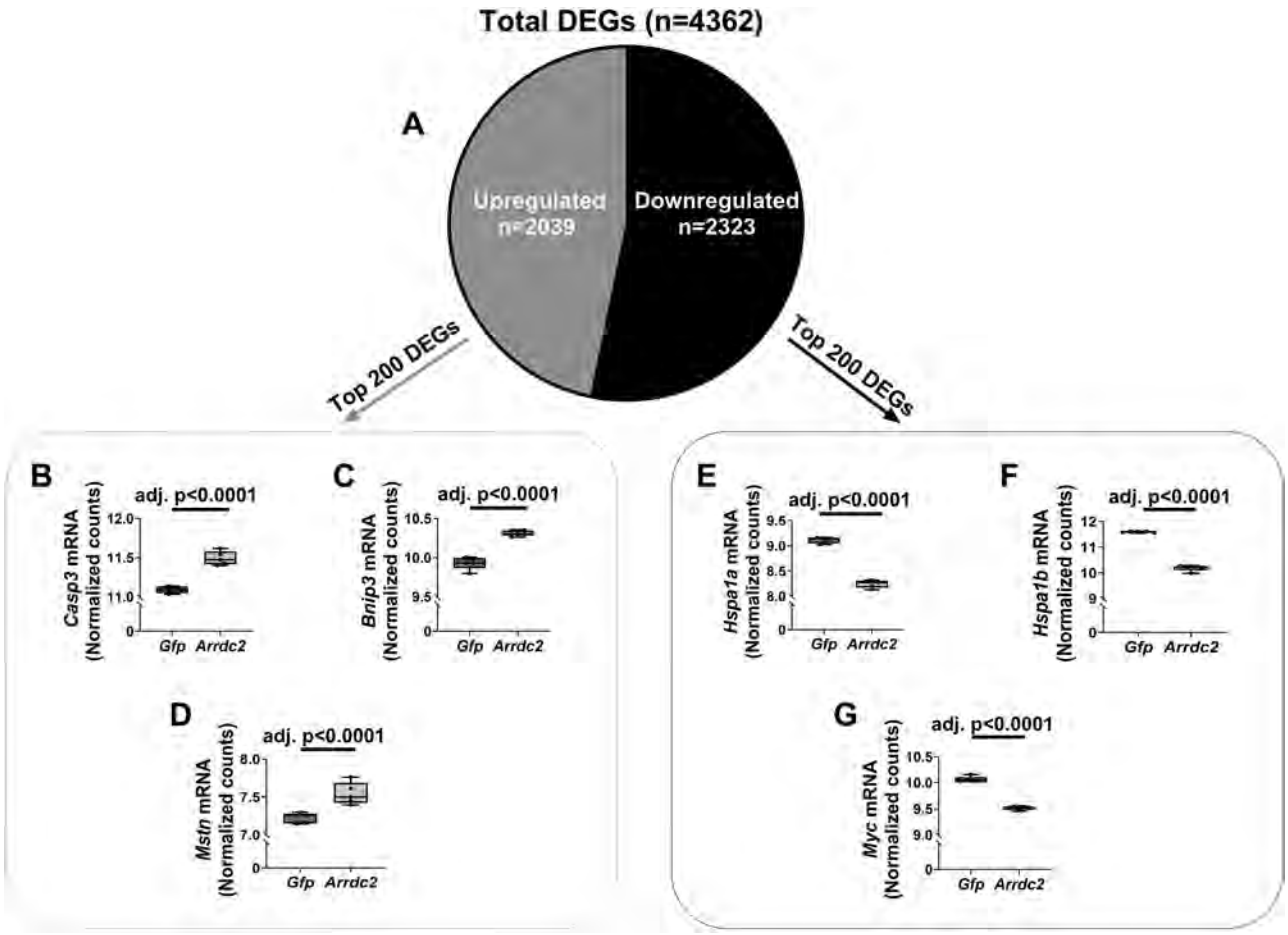

Figure 6. Arrestin domain containing 2 (*Arrdc2*) induction in C2C12 myotubes alters the transcriptome in a manner consistent with disuse atrophy. *A*: number of differentially expressed genes (DEGs) in myotubes overexpressing *Arrdc2* compared with myotubes expressing *Gfp* only at 48-h post transfection were determined by RNA sequencing analysis ($n = 5$/group; adj. P value < 0.05). *B–D*: selected transcripts associated with disuse atrophy from the top 200 most differentially expressed upregulated genes. The normalized counts for caspase-3 (*Casp*3, *B*), BCL2 interacting protein 3 (*Bnip3*, *C*), and myostatin (*Mstn*, *D*) mRNAs. *E–G*: selected transcripts associated with disuse atrophy from the top 200 most differentially expressed downregulated genes. The normalized counts for heat shock protein 70 kDa (*Hspa1a*, *E*), *Hspa1b* (*F*), and *Myc* (*G*) mRNAs. All gene counts were normalized using DESeq2. Data are presented as individual data points superimposed on box-and-whisker plots. *P* values for each comparison are shown on each panel.

(51–53). The mRNA contents of 51 genes encoding subunits of the ribosome (mitochondrial, large, small, and stalk components) were also lower in *Arrdc2* expressing myotubes (Fig. 8*H*). Analysis of the top 500 downregulated genes by adjusted *P* value using LISA predicted MYC, MYCN, sphingolipid transporter 1 (SPNS1), bromodomain-containing protein 4 (BRD4), and transcription elongation factor SPT5 (SUPT5H) to influence the downregulated gene set (Fig. 8*I*; Supplemental Table S7).

Myotube Diameter Is Thinner after 24 h of Arrdc2 Induction despite a Gene Expression Signature That Differs from 48 h

To determine the temporal relationship of changes to the transcriptome observed 48-h post-*Arrdc2* transfection to the onset of thinner myotubes, we measured myotube diameter and content of several of the identified DEGs from Figs. 7 to 9 at 24-h posttransfection. Similar to 48 h, the diameter of myotubes overexpressing *Arrdc2* was 17% thinner than the diameter of *Gfp* control myotubes 24-h posttransfection ($P = 0.0114$, Fig. 9*A*). Unlike the 48-h gene expression data, the mRNA contents of *Mafbx* ($P = 0.2632$, Fig. 9*B*), *Myog* ($P = 0.0674$, Fig. 9*C*), *Redd1* ($P = 0.7261$, Fig. 9*D*), *Bnip3* ($P = 0.7106$, Fig. 9*E*), and *Mstn* ($P = 0.2534$, Fig. 9*F*) were not different between conditions at the 24-h posttransfection time point. Once again, *Murf1* mRNA content was unchanged ($P = 0.2078$, Fig. 9*G*). Consistent with the 48-h data, *Redd2* mRNA was higher whereas *Hspa1a* mRNA content was significantly lower in *Arrdc2* expressing myotubes 24-h posttransfection ($P = 0.0399$ and $P < 0.0001$, respectively; Fig. 9, *H* and *I*).

DISCUSSION

Changes to the skeletal muscle gene expression signature contribute to the loss of skeletal muscle mass in response to disuse. Although the loss of skeletal muscle is debilitating, the consequences from muscle loss are worse in the elderly than in young individuals. Our data show that *Arrdc2* mRNA content is rapidly and sustainably induced in response to disuse, with the *Arrdc2* induction significantly more pronounced in aged muscle. We also show that increasing

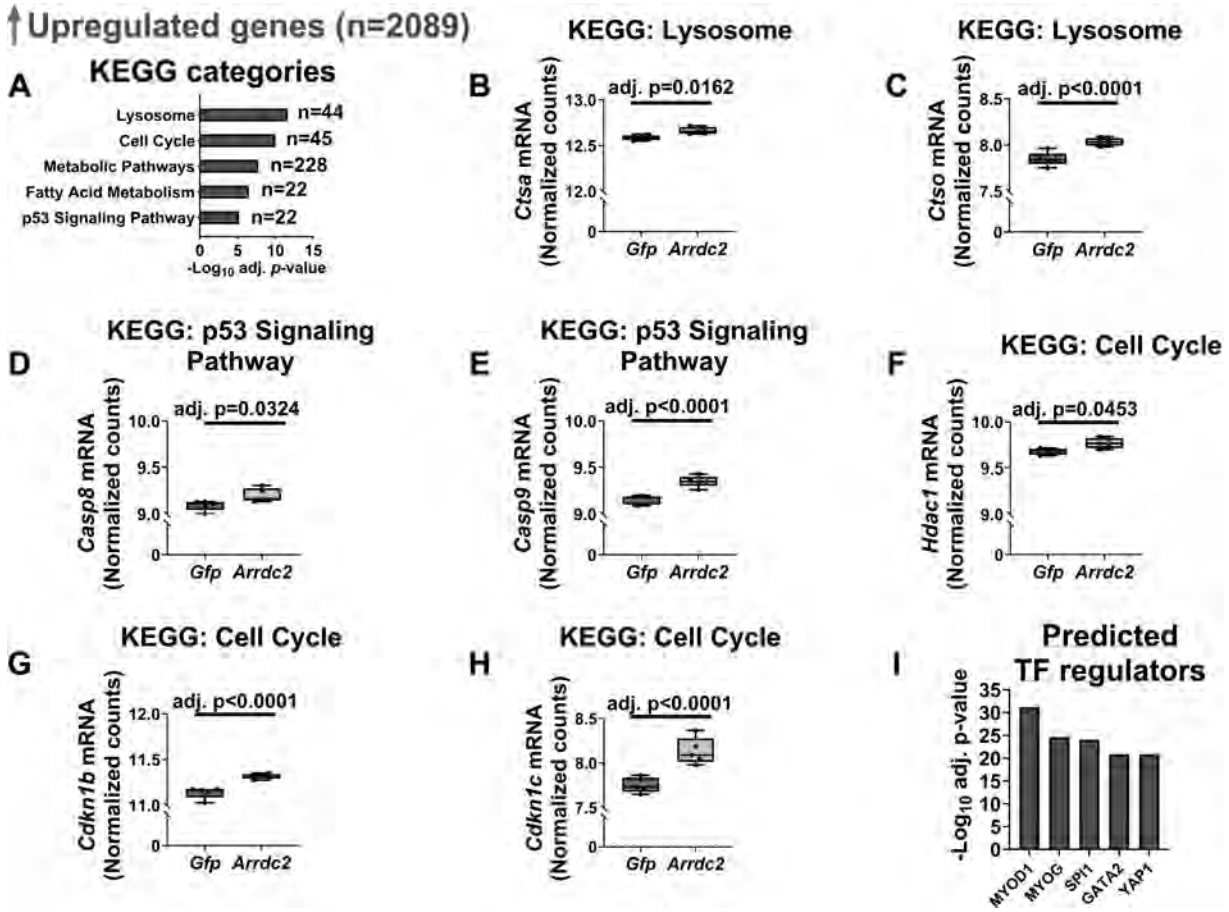

Figure 7. Functional categories of the upregulated genes in C2C12 myotubes in response to arrestin domain containing 2 (*Arrdc2*) induction. *A*: Kyoto Encyclopedia of Genes and Genomes (KEGG) categories associated with differentially expressed upregulated genes between myotubes overexpressing *Arrdc2* compared with myotubes expressing *Gfp* at 48-h posttransfection ($n = 5$/group; adj. P value < 0.05). The normalized counts for cathepsin A (*Ctsa*, *B*), cathepsin O (*Ctso*, *C*), caspase-8 (*Casp8*, *D*), *Casp9* (*E*), histone deacetylase 1 (*Hdac1*, *F*), cyclin-dependent kinase inhibitor 1B/p27 (*Cdkn1b*, *G*), and cyclin-dependent kinase inhibitor 1C/p57 (*Cdkn1c*, *H*) mRNAs were determined by RNA sequencing analysis. *I*: transcription factors predicted to influence the *Arrdc2*-mediated upregulated genes using LISA software. All gene counts were normalized using DESeq2. Data are presented as individual data points superimposed on box-and-whisker plots. *P* values for each comparison are shown on each panel.

Arrdc2 expression, but not its family member *Arrdc3*, is sufficient to produce thinner myotubes in vitro, thereby identifying a potentially novel factor contributing to disuse atrophy, particularly in aged muscle. The smaller diameter in *Arrdc2* overexpressing myotubes coincides with changes to the muscle gene expression profile, with several of those *Arrdc2*-induced directional changes also occurring in response to muscle disuse. Overall, these data identify a novel factor regulating muscle fiber size with direct implications to disuse atrophy, especially in the aged muscle.

The transcriptomic changes coinciding with the thinner *Arrdc2* overexpressing myotubes suggest ARRDC2 regulates fiber size in part through changes in gene transcription. Indeed, several of the identified genes such as *Mafbx*, *Mstn*, and *Redd1/2* are implicated in processes contributing to the loss of muscle mass in response to disuse (38, 54, 55). In addition, several mRNAs encoding for caspase and cathepsin proteases (e.g., *Casp3/8/9*, *Ctsa*, *Ctso)* were also greater in *Arrdc2* expressing myotubes, which would be consistent with an atrophy profile as caspases cleave actomyosin fragments in skeletal muscle (56) whereas cathepsins participate in protein breakdown within the lysosome (45). We also found changes to the expression of genes that may limit ribosome biogenesis and function (e.g., *Cdkn1b*, *Fbl*, *Rsl24dl*), consistent with the decrease in muscle protein synthetic rates and ribosome content that occurs in response to disuse (57, 58). However, the transcriptional landscape at 48-h posttransfection may not necessarily be the cause of the thinner myotubes at that time point considering myotube diameters in *Arrdc2* overexpressing myotubes were similarly thinner at 24- and 48-h posttransfection even though the gene expression patterns differed across the time points. Therefore, it is likely that certain changes to the transcriptome initiate the thinning of myotubes, whereas the transcriptome changes observed at 48-h posttransfection may reflect a transcriptional landscape that could promote further myotube atrophy if diameter was measured at time points exceeding 48 h. It is also worth noting several genes identified by RNA sequencing had a relatively small fold change. Whether those smaller fold changes increase in magnitude with longer *Arrdc2* induction (i.e., >48 h) needs to be assessed but is possible since the magnitude of *Redd2* induction increased with longer *Arrdc2* induction (i.e., Fig. 9*H* vs. Fig. 5*E*). The consequences of long-term *Arrdc2* induction during disuse

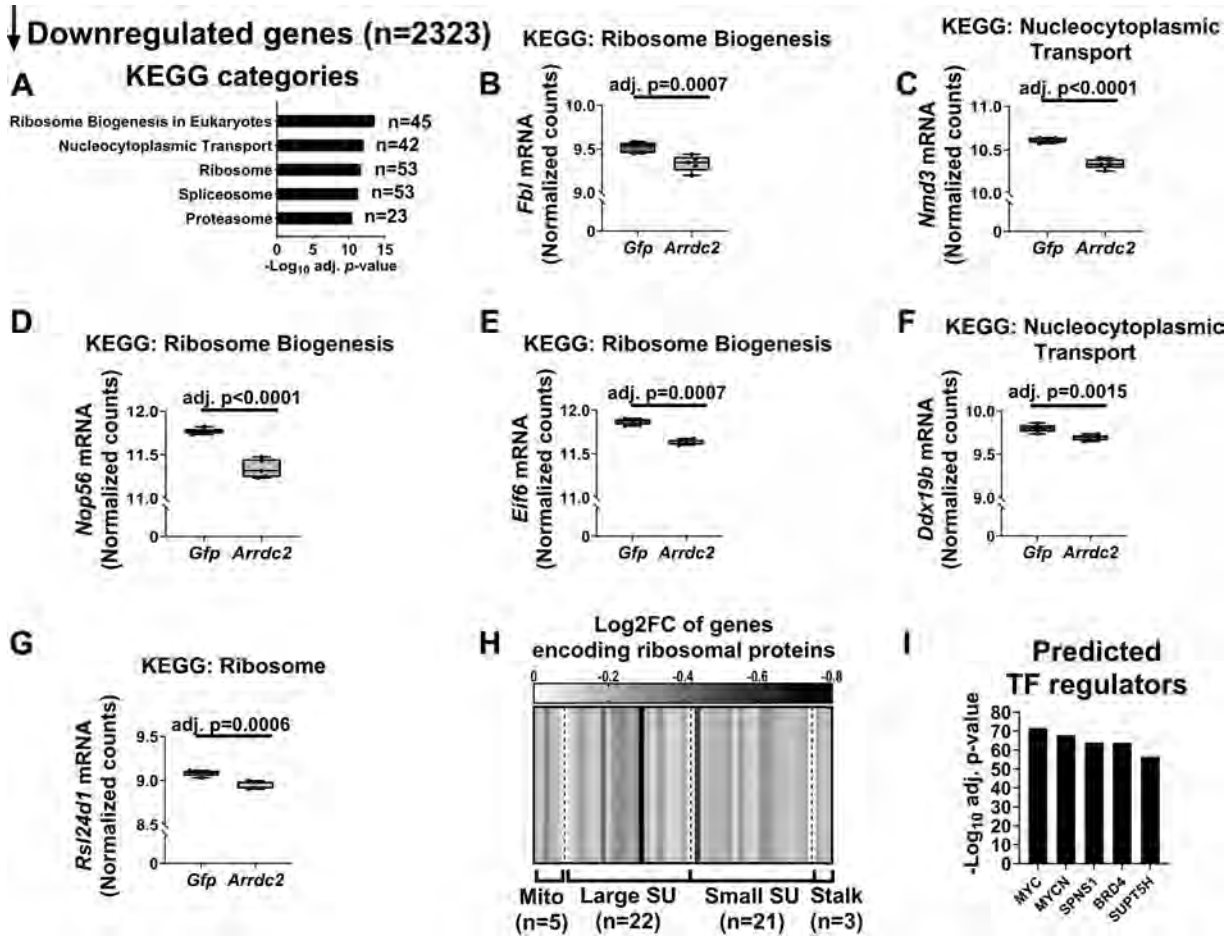

Figure 8. Functional categories of the downregulated genes in C2C12 myotubes in response to arrestin domain containing 2 (*Arrdc2*) induction. *A*: Kyoto Encyclopedia of Genes and Genomes (KEGG) categories associated with differentially expressed downregulated genes between myotubes overexpressing *Arrdc2* compared with myotubes expressing *Gfp* at 48-h posttransfection ($n = 5$/group; adj. *P* value <0.05). The normalized counts of fibrillarin (*Fbl*, *B*), NMD3 ribosome export adaptor (*Nmd3*, *C*), nucleolar protein 5A (*Nop56*, *D*), eukaryotic initiation factor 6 (*Eif6*, *E*), DEAD-box helicase 19B (*Ddx19b*, *F*), and ribosomal L24 domain containing 1 (*Rsl24d1*, *G*) mRNAs were determined by RNA sequencing analysis. *H*: heat map comprising the downregulated genes encoding ribosomal protein subunits. *I*: transcription factors predicted to influence the *Arrdc2*-mediated downregulated genes using LISA software. All gene counts were normalized using DESeq2. Data are presented as individual data points superimposed on box-and-whisker plots. *P* values for each comparison are shown on each panel.

(i.e., 7 days of unloading) on myofiber cross-sectional area and the transcriptional landscape will require muscle-specific knockout models.

The *Arrdc2*-mediated changes to myotube diameter and gene expression likely occur via a functional PPxY motif as ARRDC2 is predicted to interact with WW domain-containing proteins. Although ARRDC3 also contains a PPxY motif, differences in the amino acid at the x-position of the PPxY motifs in ARRDC2 versus ARRDC3 may partially explain why *Arrdc2*, but not *Arrdc3*, overexpression altered myotube diameter and gene expression in muscle cells as the x-position amino acid partially determines affinity for WW domain proteins (34). Specifically, one of the conserved PPxY motifs across human, rat, and mouse in the ARRDC2 amino acid sequence encodes glutamic acid in the x-position, whereas the x-position within the PPxY motif of ARRDC3 encodes leucine. Alternatively, it could be the relative expression level of WW domain-containing proteins in muscle cells versus other cell types that determine potential interactions with ARRDC2/ARRDC3 and subsequent functional effects. Indeed, our STRING analysis suggests ARRDC2 interacts with the NEDD4 subfamily of HECT domain E3 ligases, with the two highest predicted transcription factors influencing the upregulated gene set being MYOD1 and MYOG, whose activity can be positively regulated by NEDD4-mediated degradation of PAX7 (35). Likewise, the highest predicted transcription factors influencing the downregulated gene set were the MYC family proteins, which are ubiquitylated and tagged for degradation by NEDD4 (59). Another NEDD4 substrate is heat shock factor 1 (HSF1), the primary transcription factor transcribing HSP70-encoding genes including *Hspa1a* (60), which we found to be lower in *Arrdc2* overexpressing myotubes at 24-h and 48-h posttransfection. However, there are ~100 known WW domain-containing proteins (61), and ARRDC2 may interact with several of them in a time-dependent manner to influence the ARRDC2-mediated gene expression profile and/or nongenomic interactions that could influence muscle size. Future work will need to decipher the specific time-dependent mechanism(s) by which ARRDC2 regulates muscle fiber size and the gene expression

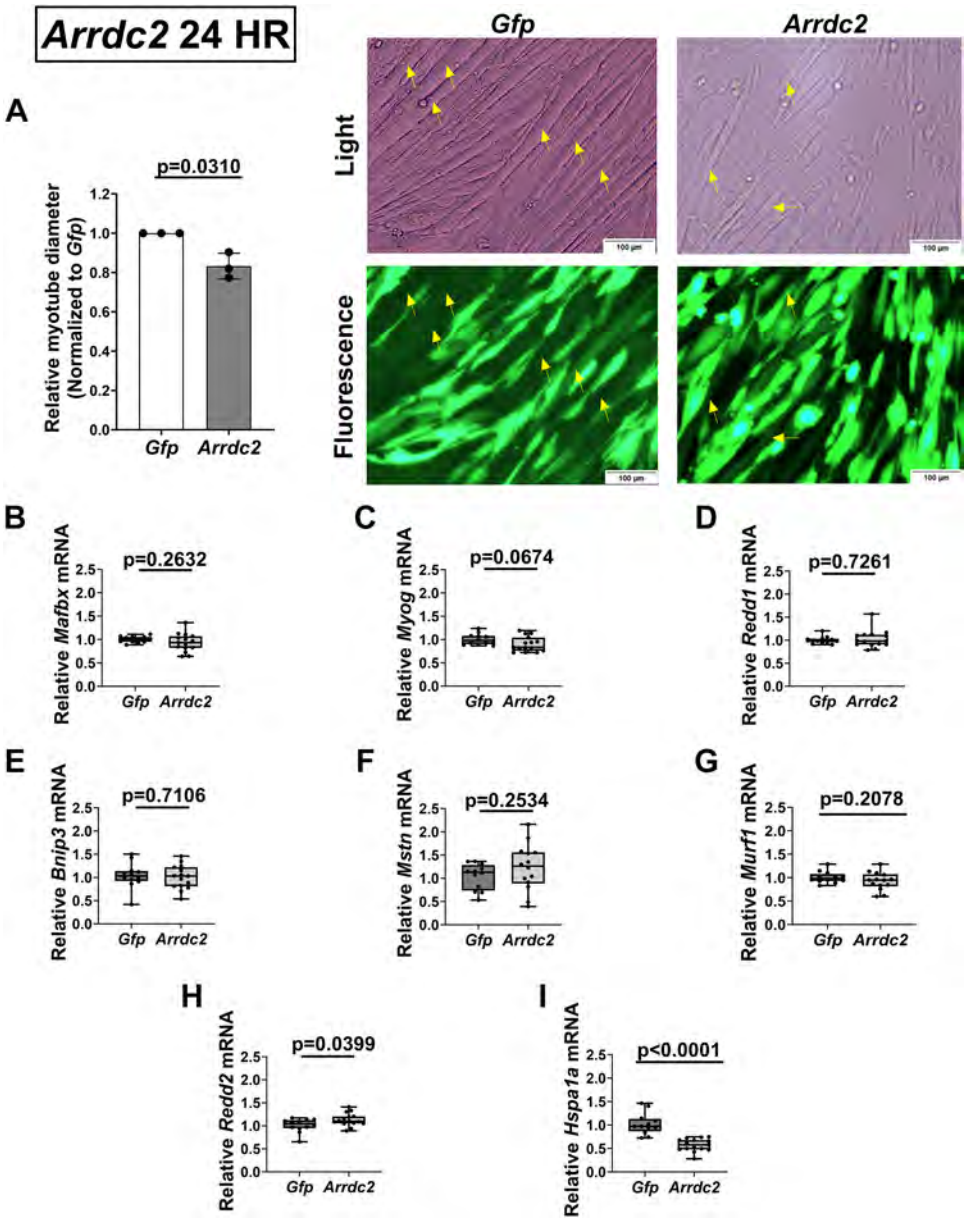

Figure 9. Changes to myotube diameter by arrestin domain containing 2 (*Arrdc2*) overexpression precede some of the changes to gene expression observed at 48 h. *A*, *left*: normalized diameter of C2C12 myotubes overexpressing *Arrdc2* or expressing *Gfp* only at 24-h posttransfection. *A*, *right*: representative light and fluorescent images of each transfection condition. Yellow arrows indicate GFP-positive, mature myotubes. $n = 139–144$ myotubes analyzed from each transfection condition generated from three independent experimental replicates. *B–I*: changes in gene expression 24-h post-*Arrdc2* transfection ($n = 15$ wells) compared with the *Gfp* transfection ($n = 12$ wells) in C2C12 myotubes. The relative mRNA content of muscle atrophy F-box (*Mafbx*, *B*), myogenin (*Myog*, *C*), regulated in development and DNA damage 1 (*Redd1*, *D*), BCL2 interacting protein 3 (*Bnip3*, *E*), myostatin (*Mstn*, *F*), muscle RING-finger protein-1 (*Murf1*, *G*), regulated in development and DNA damage 2 (*Redd2*, *H*), and *Hspa1a* (*I*) were determined by qRT-PCR. Data are relative to the *Gfp* control values and generated from three independent experimental replicates. Data analyzed by unpaired Student's *t* tests. Data are presented as three individual data points representing the normalized mean of each independent experimental replicate ± SD or individual data points superimposed on box-and-whisker plots. *P* values for each comparison are shown on each panel.

profile, including the possible role of interactions with WW domain-containing proteins. Moreover, changes in the protein levels of the mRNAs altered by *Arrdc2* induction should also be verified in future work.

Our findings show the magnitude of *Arrdc3* mRNA induction in response to mechanical unloading was less than *Arrdc2* mRNA, and accordingly only *Arrdc2* overexpression was sufficient to alter myotube diameter. The upstream signals regulating *Arrdc2* and *Arrdc3* transcript levels in response to changes in mechanical load are unknown but may be regulated by similar mechanosensitive transcriptional factors since their gene contents are inversely related to the magnitude of mechanical load placed on the muscle (at least up to normal ambulatory levels). A possible pathway regulating *Arrdc2* and *Arrdc3* expression is the mechanically sensitive Integrin signaling pathway as overexpression of transcription factors downstream of Integrin such as H-Ras, c-Src, c-Myc, and β-catenin all lowered *Arrdc3* mRNA content in human epithelial cells (62). In addition, mechanically sensitive transcription factors such as FOXO3, FOXO4, and Mothers against decapentaplegic homolog 2 (SMAD2) are known regulators of atrophy-inducing gene programs (37, 63) and their transcriptional activity can be negatively regulated by Integrin signaling (64). Analysis of the *Arrdc2* and *Arrdc3* DNA sequences using EnhancerDB identified putative FOXO3, FOXO4, and SMAD2 binding sites in the promoters of both *Arrdc2* and *Arrdc3* genes (Supplemental Table S8). Therefore, it is possible the activity of mechanically sensitive transcription factor(s) such as FOXO3, FOXO4, and SMAD2 contribute to the regulation of *Arrdc2* and *Arrdc3* mRNA content in response to changes in mechanical load.

Therapeutically, we show that *Arrdc2* mRNA content can be maintained at low values in both young and aged muscle

if mechanical load reaches or exceeds ambulatory levels. Practically, this means applying a mechanical load to the muscle during a period of disuse may help mitigate the atrophy in part by preventing/limiting induction of *ARRDC2*. This is particularly relevant for the elderly as the *Arrdc2* mRNA induction in aged mouse muscle was significantly more pronounced compared with young mouse muscle. Moreover, if traditional modalities of mechanical overload (e.g., resistance exercise) are possible, our data demonstrate that high force contractions are best at maintaining low *Arrdc2* mRNA as values in contracted muscles were lower than normal ambulatory levels in both young and aged mice. However, traditional modalities of mechanical overload are not an option if the person is unconscious or bedridden. Under those circumstances, our data show that a mechanical load equivalent to normal ambulation will keep *Arrdc2* mRNA levels low in both young and aged mouse muscle. Therefore, electromyostimulation at stimulation frequencies that evoke muscle forces equivalent to normal ambulation may maintain low *ARRDC2* mRNA levels in humans. Moreover, electromyostimulation is prescribed clinically to attenuate muscle atrophy because it is safe, effective, and feasible, particularly in the elderly (65). The application of electromyostimulation at higher stimulation frequencies to elicit more forceful contractions and a more pronounced suppression of *ARRDC2* mRNA in humans may extend to individuals that can tolerate those contractions (e.g., spinal cord injury patients) without the risk of pain (66).

In conclusion, our data show *Arrdc2* is a novel regulator of muscle size with direct implications to disuse muscle atrophy, particularly in aged muscle. In addition, our data show *Arrdc2* mRNA content is related to the degree of mechanical load placed on the muscle. Importantly, aged muscle retains the ability to lower *Arrdc2* mRNA content when unloaded muscle is returned to normal ambulation, and high force contractions in aged muscle can reduce *Arrdc2* mRNA to levels below normal ambulation. Although this work provides a baseline understanding of the role of *Arrdc2/ARRDC2* in the regulation of skeletal muscle size, future work should validate changes in ARRDC2 at the protein level following disuse, given the poor association between some mRNAs and the proteins they encode. Potential future investigations may include identification of specific ARRDC2 protein binding partners to define the downstream signals regulating muscle fiber size, as well as using loss-of-function approaches (i.e., *Arrdc2* knockout) to define the contribution of ARRDC2 protein to the atrophy induced by disuse, especially in aged muscle.

DATA AVAILABILITY

The data that support the findings of this study are available at GEO or are available from the corresponding author upon reasonable request.

SUPPLEMENTAL DATA

Supplemental Tables S1–S8 and Supplemental Fig. S1: https://doi.org/10.17632/d2rc6c9bcs.1.

ACKNOWLEDGMENTS

Graphical abstract was created using Biorender and published with permission. We would also like to thank the authors that produced the publicly available RNA sequencing datasets used in our analyses.

GRANTS

This work was supported in part by NIH Grants R03AG073445 (to B.S.G.), R15AR069913 (to N.P.G.), and P20GM125503, as well as a seed grant from the Institute for Successful Longevity at Florida State University (to B.S.G.).

DISCLOSURES

No conflicts of interest, financial or otherwise, are declared by the authors.

AUTHOR CONTRIBUTIONS

G.R.L. and B.S.G. conceived and designed research; G.R.L., A.R.C., N.P.G., R.J.T., and C.V. performed experiments; G.R.L., A.R.C., N.P.G., R.J.T., and C.V. analyzed data; G.R.L., A.R.C., N.P.G., R.J.T., and B.S.G. interpreted results of experiments; G.R.L. prepared figures; G.R.L. drafted manuscript; G.R.L., A.R.C., N.P.G., R.J.T., C.V., and B.S.G. edited and revised manuscript; G.R.L., A.R.C., N.P.G., R.J.T., C.V., and B.S.G. approved final version of manuscript.

REFERENCES

1. **Li R**, **Xia J**, **Zhang XI**, **Gathirua-Mwangi WG**, **Guo J**, **Li Y**, **McKenzie S**, **Song Y.** Associations of muscle mass and strength with all-cause mortality among US older adults. *Med Sci Sports Exerc* 50: 458–467, 2018. doi:10.1249/MSS.0000000000001448.
2. **Hanna L**, **Nguo K**, **Furness K**, **Porter J**, **Huggins CE.** Association between skeletal muscle mass and quality of life in adults with cancer: a systematic review and meta-analysis. *J Cachexia Sarcopenia Muscle* 13: 839–857, 2022. doi:10.1002/jcsm.12928.
3. **Atherton PJ**, **Greenhaff PL**, **Phillips SM**, **Bodine SC**, **Adams CM**, **Lang CH.** Control of skeletal muscle atrophy in response to disuse: clinical/preclinical contentions and fallacies of evidence. *Am J Physiol Endocrinol Physiol* 311: E594–E604, 2016. doi:10.1152/ajpendo.00257.2016.
4. **Evans WJ.** Skeletal muscle loss: cachexia, sarcopenia, and inactivity. *Am J Clin Nutr* 91: 1123S–1127S, 2010. doi:10.3945/ajcn.2010.28608A.
5. **Tanner RE**, **Brunker LB**, **Agergaard J**, **Barrows KM**, **Briggs RA**, **Kwon OS**, **Young LM**, **Hopkins PN**, **Volpi E**, **Marcus RL**, **LaStayo PC**, **Drummond MJ.** Age-related differences in lean mass, protein synthesis and skeletal muscle markers of proteolysis after bed rest and exercise rehabilitation. *J Physiol* 593: 4259–4273, 2015. doi:10.1113/JP270699.
6. **Hvid L**, **Aagaard P**, **Justesen L**, **Bayer ML**, **Andersen JL**, **Ørtenblad N**, **Kjaer M**, **Suetta C.** Effects of aging on muscle mechanical function and muscle fiber morphology during short-term immobilization and subsequent retraining. *J Appl Physiol (1985)* 109: 1628–1634, 2010. doi:10.1152/japplphysiol.00637.2010.
7. **Suetta C**, **Hvid LG**, **Justesen L**, **Christensen U**, **Neergaard K**, **Simonsen L**, **Ortenblad N**, **Magnusson SP**, **Kjaer M**, **Aagaard P.** Effects of aging on human skeletal muscle after immobilization and retraining. *J Appl Physiol (1985)* 107: 1172–1180, 2009. doi:10.1152/japplphysiol.00290.2009.
8. **Baehr LM**, **West DWD**, **Marshall AG**, **Marcotte GR**, **Baar K**, **Bodine SC.** Muscle-specific and age-related changes in protein synthesis and protein degradation in response to hindlimb unloading in rats. *J Appl Physiol (1985)* 122: 1336–1350, 2017. doi:10.1152/japplphysiol.00703.2016.

9. **Leeuwenburgh C**, **Gurley CM**, **Strotman BA**, **Dupont-Versteegden EE.** Age-related differences in apoptosis with disuse atrophy in soleus muscle. *Am J Physiol Regul Integr Comp Physiol* 288: R1288–R1296, 2005. doi:10.1152/ajpregu.00576.2004.
10. **Kelleher AR**, **Pereira SL**, **Jefferson LS**, **Kimball SR.** REDD2 expression in rat skeletal muscle correlates with nutrient-induced activation of mTORC1: responses to aging, immobilization, and remobilization. *Am J Physiol Endocrinol Physiol* 308: E122–E129, 2015. doi:10.1152/ajpendo.00341.2014.
11. **Alvarez CE.** On the origins of arrestin and rhodopsin. *BMC Evol Biol* 8: 222, 2008. doi:10.1186/1471-2148-8-222.
12. **Gordon BS**, **Rossetti ML**, **Eroshkin AM.** Arrdc2 and Arrdc3 elicit divergent changes in gene expression in skeletal muscle following anabolic and catabolic stimuli. *Physiol Genomics* 51: 208–217, 2019. doi:10.1152/physiolgenomics.00007.2019.
13. **Wedegaertner H**, **Pan W-A**, **Gonzalez CC**, **Gonzalez DJ**, **Trejo J.** The α-arrestin ARRDC3 is an emerging multifunctional adaptor protein in cancer. *Antioxid Redox Signal* 36: 1066–1079, 2022. doi:10.1089/ars.2021.0193.
14. **Watt KI**, **Turner BJ**, **Hagg A**, **Zhang X**, **Davey JR**, **Qian H**, **Beyer C**, **Winbanks CE**, **Harvey KF**, **Gregorevic P.** The Hippo pathway effector YAP is a critical regulator of skeletal muscle fibre size. *Nat Commun* 6: 6048, 2015. doi:10.1038/ncomms7048.
15. **Han S-O**, **Kommaddi RP**, **Shenoy SK.** Distinct roles for β-arrestin2 and arrestin-domain-containing proteins in β2 adrenergic receptor trafficking. *EMBO Rep* 14: 164–171, 2013. doi:10.1038/embor.2012.187.
16. **Rosa-Caldwell ME**, **Lim S**, **Haynie WA**, **Brown JL**, **Deaver JW**, **Morena Da Silva F**, **Jansen LT**, **Lee DE**, **Wiggs MP**, **Washington TA**, **Greene NP.** Female mice may have exacerbated catabolic signalling response compared to male mice during development and progression of disuse atrophy. *J Cachexia Sarcopenia Muscle* 12: 717–730, 2021. doi:10.1002/jcsm.12693.
17. **Zhang X**, **Trevino MB**, **Wang M**, **Gardell SJ**, **Ayala JE**, **Han X**, **Kelly DP**, **Goodpaster BH**, **Vega RB**, **Coen PM.** Impaired mitochondrial energetics characterize poor early recovery of muscle mass following hind limb unloading in old mice. *J Gerontol A Biol Sci Med Sci* 73: 1313–1322, 2018. doi:10.1093/gerona/gly051.
18. **Standley RA**, **Distefano G**, **Trevino MB**, **Chen E**, **Narain NR**, **Greenwood B**, **Kondakci G**, **Tolstikov VV**, **Kiebish MA**, **Yu G**, **Qi F**, **Kelly DP**, **Vega RB**, **Coen PM**, **Goodpaster BH.** Skeletal muscle energetics and mitochondrial function are impaired following 10 days of bed rest in older adults. *J Gerontol A Biol Sci Med Sci* 75: 1744–1753, 2020. doi:10.1093/gerona/glaa001.
19. **Laskin GR**, **Gordon BS.** The influence of nutrients on mechanical overload-induced changes to skeletal muscle mRNA content. *Physiol Genomics* 54: 360–369, 2022. doi:10.1152/physiolgenomics.00075.2022.
20. **Abmayr SM**, **Pavlath GK.** Myoblast fusion: lessons from flies and mice. *Development* 139: 641–656, 2012. doi:10.1242/dev.068353.
21. **Szklarczyk D**, **Kirsch R**, **Koutrouli M**, **Nastou K**, **Mehryary F**, **Hachilif R**, **Gable AL**, **Fang T**, **Doncheva NT**, **Pyysalo S**, **Bork P**, **Jensen LJ**, **von Mering C.** The STRING database in 2023: protein-protein association networks and functional enrichment analyses for any sequenced genome of interest. *Nucleic Acids Res* 51: D638–D646, 2023. doi:10.1093/nar/gkac1000.
22. **Kang R**, **Zhang Y**, **Huang Q**, **Meng J**, **Ding R**, **Chang Y**, **Xiong L**, **Guo Z.** EnhancerDB: a resource of transcriptional regulation in the context of enhancers. *Database* 2019: bay141, 2019. doi:10.1093/database/bay141.
23. **Buchan DWA**, **Jones DT.** The PSIPRED Protein Analysis Workbench: 20 years on. *Nucleic Acids Res* 47: W402–W407, 2019. doi:10.1093/nar/gkz297.
24. **Kelley LA**, **Mezulis S**, **Yates CM**, **Wass MN**, **Sternberg MJE.** The Phyre2 web portal for protein modeling, prediction and analysis. *Nat Protoc* 10: 845–858, 2015. doi:10.1038/nprot.2015.053.
25. **Cramer P.** AlphaFold2 and the future of structural biology. *Nat Struct Mol Biol* 28: 704–705, 2021. doi:10.1038/s41594-021-00650-1.
26. **Dobin A**, **Davis CA**, **Schlesinger F**, **Drenkow J**, **Zaleski C**, **Jha S**, **Batut P**, **Chaisson M**, **Gingeras TR.** STAR: ultrafast universal RNA-seq aligner. *Bioinformatics* 29: 15–21, 2013. doi:10.1093/bioinformatics/bts635.
27. **Love MI**, **Huber W**, **Anders S.** Moderated estimation of fold change and dispersion for RNA-seq data with DESeq2. *Genome Biol* 15: 550, 2014. doi:10.1186/s13059-014-0550-8.
28. **Huang DW**, **Sherman BT**, **Tan Q**, **Collins JR**, **Alvord WG**, **Roayaei J**, **Stephens R**, **Baseler MW**, **Lane HC**, **Lempicki RA.** The DAVID Gene Functional Classification Tool: a novel biological module-centric algorithm to functionally analyze large gene lists. *Genome Biol* 8: R183, 2007. doi:10.1186/gb-2007-8-9-r183.
29. **Englund DA**, **Figueiredo VC**, **Dungan CM**, **Murach KA**, **Peck BD**, **Petrosino JM**, **Brightwell CR**, **Dupont AM**, **Neal AC**, **Fry CS**, **Accornero F**, **McCarthy JJ**, **Peterson CA.** Satellite cell depletion disrupts transcriptional coordination and muscle adaptation to exercise. *Function (Oxf)* 2: zqaa033, 2021. doi:10.1093/function/zqaa033.
30. **Murach KA**, **Liu Z**, **Jude B**, **Figueiredo VC**, **Wen Y**, **Khadgi S**, **Lim S**, **Morena da Silva F**, **Greene NP**, **Lanner JT**, **McCarthy JJ**, **Vechetti IJ**, **von Walden F.** Multi-transcriptome analysis following an acute skeletal muscle growth stimulus yields tools for discerning global and MYC regulatory networks. *J Biol Chem* 298: 102515, 2022. doi:10.1016/j.jbc.2022.102515.
31. **Qin Q**, **Fan J**, **Zheng R**, **Wan C**, **Mei S**, **Wu Q**, **Sun H**, **Brown M**, **Zhang J**, **Meyer CA**, **Liu XS.** Lisa: inferring transcriptional regulators through integrative modeling of public chromatin accessibility and ChIP-seq data. *Genome Biol* 21: 32, 2020. doi:10.1186/s13059-020-1934-6.
32. **Nagpal P**, **Plant PJ**, **Correa J**, **Bain A**, **Takeda M**, **Kawabe H**, **Rotin D**, **Bain JR**, **Batt JAE.** The ubiquitin ligase Nedd4-1 participates in denervation-induced skeletal muscle atrophy in mice. *PLoS One* 7: e46427, 2012. doi:10.1371/journal.pone.0046427.
33. **Koncarevic A**, **Jackman RW**, **Kandarian SC.** The ubiquitin-protein ligase Nedd4 targets Notch1 in skeletal muscle and distinguishes the subset of atrophies caused by reduced muscle tension. *FASEB J* 21: 427–437, 2007. doi:10.1096/fj.06-6665com.
34. **Hatstat AK**, **Pupi MD**, **McCafferty DG.** Predicting PY motif-mediated protein-protein interactions in the Nedd4 family of ubiquitin ligases. *PLoS One* 16: e0258315, 2021. doi:10.1371/journal.pone.0258315.
35. **Bustos F**, **de la Vega E**, **Cabezas F**, **Thompson J**, **Cornelison DDW**, **Olwin BB**, **Yates JR**, **Olguín HC.** NEDD4 regulates PAX7 levels promoting activation of the differentiation program in skeletal muscle precursors. *Stem Cells* 33: 3138–3151, 2015. doi:10.1002/stem.2125.
36. **Kim B-G**, **Lee J-H**, **Yasuda J**, **Ryoo H-M**, **Cho J-Y.** Phospho-Smad1 modulation by nedd4 e3 ligase in BMP/TGF-β signaling. *J Bone Miner Res* 26: 1411–1424, 2011. [Erratum in *J Bone Miner Res* 27: 1437, 2012]. doi:10.1002/jbmr.348.
37. **Sandri M**, **Sandri C**, **Gilbert A**, **Skurk C**, **Calabria E**, **Picard A**, **Walsh K**, **Schiaffino S**, **Lecker SH**, **Goldberg AL.** Foxo transcription factors induce the atrophy-related ubiquitin ligase atrogin-1 and cause skeletal muscle atrophy. *Cell* 117: 399–412, 2004. doi:10.1016/s0092-8674(04)00400-3.
38. **Kelleher AR**, **Kimball SR**, **Dennis MD**, **Schilder RJ**, **Jefferson LS.** The mTORC1 signaling repressors REDD1/2 are rapidly induced and activation of p70S6K1 by leucine is defective in skeletal muscle of an immobilized rat hindlimb. *Am J Physiol Endocrinol Physiol* 304: E229–E236, 2013. doi:10.1152/ajpendo.00409.2012.
39. **Talbert EE**, **Smuder AJ**, **Min K**, **Kwon OS**, **Powers SK.** Calpain and caspase-3 play required roles in immobilization-induced limb muscle atrophy. *J Appl Physiol (1985)* 114: 1482–1489, 2013. doi:10.1152/japplphysiol.00925.2012.
40. **Yamashita S-I**, **Kyuuma M**, **Inoue K**, **Hata Y**, **Kawada R**, **Yamabi M**, **Fujii Y**, **Sakagami J**, **Fukuda T**, **Furukawa K**, **Tsukamoto S**, **Kanki T.** Mitophagy reporter mouse analysis reveals increased mitophagy activity in disuse-induced muscle atrophy. *J Cell Physiol* 236: 7612–7624, 2021. doi:10.1002/jcp.30404.
41. **Gustafsson T**, **Osterlund T**, **Flanagan JN**, **von Waldén F**, **Trappe TA**, **Linnehan RM**, **Tesch PA.** Effects of 3 days unloading on molecular regulators of muscle size in humans. *J Appl Physiol (1985)* 109: 721–727, 2010. doi:10.1152/japplphysiol.00110.2009.
42. **Hanson AM**, **Young MH**, **Harrison BC**, **Zhou X**, **Han HQ**, **Stodieck LS**, **Ferguson VL.** Inhibiting myostatin signaling partially mitigates structural and functional adaptations to hindlimb suspension in mice. *NPJ Microgravity* 9: 2–11, 2023. doi:10.1038/s41526-022-00233-4.
43. **Senf SM**, **Dodd SL**, **McClung JM**, **Judge AR.** Hsp70 overexpression inhibits NF-κB and Foxo3a transcriptional activities and prevents skeletal muscle atrophy. *FASEB J* 22: 3836–3845, 2008. doi:10.1096/fj.08-110163.

44. **Rozhkov SV**, **Sharlo KA**, **Mirzoev TM**, **Shenkman BS.** Temporal changes in the markers of ribosome biogenesis in rat soleus muscle under simulated microgravity. *Acta Astronautica* 186: 252–258, 2021. doi:10.1016/j.actaastro.2021.05.036.
45. **Bechet D**, **Tassa A**, **Taillandier D**, **Combaret L**, **Attaix D.** Lysosomal proteolysis in skeletal muscle. *Int J Biochem Cell Biol* 37: 2098–2114, 2005. doi:10.1016/j.biocel.2005.02.029.
46. **Belizário JE**, **Lorite MJ**, **Tisdale MJ.** Cleavage of caspases-1, -3, -6, -8 and -9 substrates by proteases in skeletal muscles from mice undergoing cancer cachexia. *Br J Cancer* 84: 1135–1140, 2001. doi:10.1054/bjoc.2001.1700.
47. **Beharry AW**, **Sandesara PB**, **Roberts BM**, **Ferreira LF**, **Senf SM**, **Judge AR.** HDAC1 activates FoxO and is both sufficient and required for skeletal muscle atrophy. *J Cell Sci* 127: 1441–1453, 2014. doi:10.1242/jcs.136390.
48. **Nader GA**, **McLoughlin TJ**, **Esser KA.** mTOR function in skeletal muscle hypertrophy: increased ribosomal RNA via cell cycle regulators. *Am J Physiol Cell Physiol* 289: C1457–C1465, 2005. doi:10.1152/ajpcell.00165.2005.
49. **Bai B**, **Moore HM**, **Laiho M.** CRM1 and its ribosome export adaptor NMD3 localize to the nucleolus and affect rRNA synthesis. *Nucleus* 4: 315–325, 2013. doi:10.4161/nucl.25342.
50. **Chaillou T**, **Kirby TJ**, **McCarthy JJ.** Ribosome biogenesis: emerging evidence for a central role in the regulation of skeletal muscle mass. *J Cell Physiol* 229: 1584–1594, 2014. doi:10.1002/jcp.24604.
51. **Brina D**, **Miluzio A**, **Ricciardi S**, **Biffo S.** eIF6 anti-association activity is required for ribosome biogenesis, translational control and tumor progression. *Biochim Biophys Acta* 1849: 830–835, 2015. doi:10.1016/j.bbagrm.2014.09.010.
52. **Mikhailova T**, **Shuvalova E**, **Ivanov A**, **Susorov D**, **Shuvalov A**, **Kolosov PM**, **Alkalaeva E.** RNA helicase DDX19 stabilizes ribosomal elongation and termination complexes. *Nucleic Acids Res* 45: 1307–1318, 2017. doi:10.1093/nar/gkw1239.
53. **Durand S**, **Bruelle M**, **Bourdelais F**, **Bennychen B**, **Blin-Gonthier J**, **Isaac C**, **Huyghe A**, **Martel S**, **Seyve A**, **Vanbelle C**, **Adrait A**, **Couté Y**, **Meyronet D**, **Catez F**, **Diaz J-J**, **Lavial F**, **Ricci EP**, **Ducray F**, **Gabut M.** RSL24D1 sustains steady-state ribosome biogenesis and pluripotency translational programs in embryonic stem cells. *Nat Commun* 14: 356, 2023. doi:10.1038/s41467-023-36037-7.
54. **Bodine SC**, **Baehr LM.** Skeletal muscle atrophy and the E3 ubiquitin ligases MuRF1 and MAFbx/atrogin-1. *Am J Physiol Endocrinol Physiol* 307: E469–E484, 2014. doi:10.1152/ajpendo.00204.2014.
55. **Rodriguez J**, **Vernus B**, **Chelh I**, **Cassar-Malek I**, **Gabillard JC**, **Hadj Sassi A**, **Seiliez I**, **Picard B**, **Bonnieu A.** Myostatin and the skeletal muscle atrophy and hypertrophy signaling pathways. *Cell Mol Life Sci* 71: 4361–4371, 2014. doi:10.1007/s00018-014-1689-x.
56. **Du J**, **Wang X**, **Miereles C**, **Bailey JL**, **Debigare R**, **Zheng B**, **Price SR**, **Mitch WE.** Activation of caspase-3 is an initial step triggering accelerated muscle proteolysis in catabolic conditions. *J Clin Invest* 113: 115–123, 2004. doi:10.1172/JCI18330.
57. **Glover EI**, **Phillips SM**, **Oates BR**, **Tang JE**, **Tarnopolsky MA**, **Selby A**, **Smith K**, **Rennie MJ.** Immobilization induces anabolic resistance in human myofibrillar protein synthesis with low and high dose amino acid infusion. *J Physiol* 586: 6049–6061, 2008. doi:10.1113/jphysiol.2008.160333.
58. **Figueiredo VC**, **D'Souza RF**, **Van Pelt DW**, **Lawrence MM**, **Zeng N**, **Markworth JF**, **Poppitt SD**, **Miller BF**, **Mitchell CJ**, **McCarthy JJ**, **Dupont-Versteegden EE**, **Cameron-Smith D.** Ribosome biogenesis and degradation regulate translational capacity during muscle disuse and reloading. *J Cachexia Sarcopenia Muscle* 12: 130–143, 2021. doi:10.1002/jcsm.12636.
59. **Liu PY**, **Xu N**, **Malyukova A**, **Scarlett CJ**, **Sun YT**, **Zhang XD**, **Ling D**, **Su S-P**, **Nelson C**, **Chang DK**, **Koach J**, **Tee AE**, **Haber M**, **Norris MD**, **Toon C**, **Rooman I**, **Xue C**, **Cheung BB**, **Kumar S**, **Marshall GM**, **Biankin AV**, **Liu T.** The histone deacetylase SIRT2 stabilizes Myc oncoproteins. *Cell Death Differ* 20: 503–514, 2013. doi:10.1038/cdd.2012.147.
60. **Kim E**, **Wang B**, **Sastry N**, **Masliah E**, **Nelson PT**, **Cai H**, **Liao FF.** NEDD4-mediated HSF1 degradation underlies α-synucleinopathy. *Hum Mol Genet* 25: 211–222, 2016. doi:10.1093/hmg/ddv445.
61. **Sudol M**, **McDonald CB**, **Farooq A.** Molecular insights into the WW domain of the Golabi-Ito-Hall syndrome protein PQBP1. *FEBS Lett* 586: 2795–2799, 2012. doi:10.1016/j.febslet.2012.03.041.
62. **Draheim KM**, **Chen HB**, **Tao Q**, **Moore N**, **Roche M**, **Lyle S.** ARRDC3 suppresses breast cancer progression by negatively regulating integrin beta4. *Oncogene* 29: 5032–5047, 2010. doi:10.1038/onc.2010.250.
63. **Tando T**, **Hirayama A**, **Furukawa M**, **Sato Y**, **Kobayashi T**, **Funayama A**, **Kanaji A**, **Hao W**, **Watanabe R**, **Morita M**, **Oike T**, **Miyamoto K**, **Soga T**, **Nomura M**, **Yoshimura A**, **Tomita M**, **Matsumoto M**, **Nakamura M**, **Toyama Y**, **Miyamoto T.** Smad2/3 proteins are required for immobilization-induced skeletal muscle atrophy. *J Biol Chem* 291: 12184–12194, 2016. doi:10.1074/jbc.M115.680579.
64. **Schiaffino S**, **Mammucari C.** Regulation of skeletal muscle growth by the IGF1-Akt/PKB pathway: insights from genetic models. *Skelet Muscle* 1: 4, 2011. doi:10.1186/2044-5040-1-4.
65. **Paillard T.** Muscle plasticity of aged subjects in response to electrical stimulation training and inversion and/or limitation of the sarcopenic process. *Ageing Res Rev* 46: 1–13, 2018. doi:10.1016/j.arr.2018.05.002.
66. **Arija-Blázquez A**, **Ceruelo-Abajo S**, **Díaz-Merino MS**, **Godino-Durán JA**, **Martínez-Dhier L**, **Martin JLR**, **Florensa-Vila J.** Effects of electromyostimulation on muscle and bone in men with acute traumatic spinal cord injury: a randomized clinical trial. *J Spinal Cord Med* 37: 299–309, 2014. doi:10.1179/2045772313Y.0000000142.